Fire Hazards of Lithium Batteries

James G. Quintiere, Sean B. Crowley, Richard N. Walters, Richard E. Lyon, and David Blake

February 2016

DOT/FAA/TC-TN15/17

U.S. Department of Transportation
Federal Aviation Administration

NOTICE

This document is disseminated under the sponsorship of the U.S. Department of Transportation in the interest of information exchange. The United States Government assumes no liability for the contents or use thereof. The United States Government does not endorse products or manufacturers. Trade or manufacturer's names appear herein solely because they are considered essential to the objective of this report. The findings and conclusions in this report are those of the author(s) and do not necessarily represent the views of the funding agency. This document does not constitute FAA policy. Consult the FAA sponsoring organization listed on the Technical Documentation page as to its use.

This report is available at the Federal Aviation Administration William J. Hughes Technical Center's Full-Text Technical Reports page: actlibrary.tc.faa.gov in Adobe Acrobat portable document format (PDF).

1. Report No. DOT/FAA/TC-TN15/17	2. Government Accession No.	3. Recipient's Catalog No.
4. Title and Subtitle Fire Hazards of Lithium Batteries		5. Report Date February 2016
		6. Performing Organization Code
7. Author(s) J.G. Quintiere[1], S. Crowley[2], R.N. Walters[2], R.E. Lyon[2], and D. Blake[2]		8. Performing Organization Report No.
9. Performing Organization Name and Address [1]Department of Fire Protection Engineering University of Maryland College Park, MD 20742 [2]Airport and Aircraft R&D Division Federal Aviation Administration William J. Hughes Technical Center Atlantic City International Airport, NJ 08405		10. Work Unit No. (TRAIS)
		11. Contract or Grant No.
12. Sponsoring Agency Name and Address U.S. Department of Transportation Federal Aviation Administration Northwest Mountain Region – Transport Airplane Directorate 1601 Lind Avenue, SW Renton, WA 98057		13. Type of Report and Period Covered
		14. Sponsoring Agency Code ANM-115

15. Supplementary Notes

The Federal Aviation Administration William J. Hughes Technical Center Aviation Research Division COR was Richard Walters.

16. Abstract

The fire hazard of lithium batteries carried on airplanes in passenger electronics and shipped as cargo includes the energy generated by individual cell failure, subsequent self-heating (thermal runaway), and the energy released by burning or explosion of the volatile cell components. In this study, a variety of non-rechargeable lithium metal (primary) cells and rechargeable lithium-ion (secondary) cells were heated to failure using radiant energy in a fire (cone) calorimeter and electrical resistance heating in a thermal capacitance (slug) calorimeter. In the fire calorimeter, hazard parameters were measured for several different cell chemistries over a range of electrical charge (states of charge [SOC]) and radiant heat flux, including the loss of cell mass at failure, the maximum rate of heat released in flaming combustion, the total heat released by combustion of the volatiles, and the specific heat of combustion of the cell contents. In the thermal capacitance calorimeter, the chemical energy released as heat and the cell temperature were measured as a function of the SOC and the heating rate. This report documents the results of these tests; namely, combustion energy measured for several lithium primary and secondary cells and the chemical energy released as heat during failure of a lithium-ion secondary cell. The results can be used to quantify the thermal hazard and the combustion hazard of individual electrochemical cells and cell assemblies (batteries).

17. Key Words Lithium-ion battery, Thermal runaway, Fire calorimeter	18. Distribution Statement This document is available to the U.S. public through the National Technical Information Service (NTIS), Springfield, Virginia 22161. This document is also available from the Federal Aviation Administration William J. Hughes Technical Center at actlibrary.tc.faa.gov.		
19. Security Classif. (of this report) Unclassified	20. Security Classif. (of this page) Unclassified	21. No. of Pages 50	22. Price

Form DOT F 1700.7 (8-72)   Reproduction of completed page authorized

ACKNOWLEDGEMENTS

TABLE OF CONTENTS

LIST OF FIGURES

LIST OF TABLES

LIST OF ACRONYMS

HOC	Heat of combustion
HRR	Heat release rate
LFL	Lower flammability limit
OSU	Ohio State University
PHRR	Peak heat release rate
SOC	State of charge
THR	Total heat release

EXECUTIVE SUMMARY

This report addresses the energy released during the failure of lithium and other electrochemical cells (batteries). There are two forms of energy released during failure of the lithium cell: (1) the chemical potential energy released by an internal short circuit that results in rapid heating and thermal decomposition of the cell components (thermal runaway), and (2) the combustion energy released by conflagration or explosion of the gases generated and released during thermal runaway. In this study, the first form of energy release was examined. Cell failure was initiated by radiant heating in a fire calorimeter, and the energy released by flaming combustion of the cell contents was measured using the oxygen consumption method. Cell failure was also initiated by electrical resistance heating in a thermal capacitance calorimeter, and the chemical energy released as heat was computed from the temperature rise of the device. Measurements were made over a range of electrical charges (e.g., states of charge [SOC]) for rechargeable cells and over a range of radiant heat flux (fire calorimeter) or electrical heating rates (thermal capacitance calorimeter). The following observations were made:

- The ejected mass of the cell contents at failure is approximately proportional to the electric charge for a given voltage.

- The energy released as heat during the failure of an 18650 lithium-ion cell is roughly proportional to the electric charge times the voltage, which is the chemical potential free energy, ΔG.

- The duration of energy release for electrochemical cells heated to failure is very short (approximately 2 seconds).

- Surface temperatures of 18650 lithium-ion cells and ejected contents heated to failure increased with SOC and were as high as 1000ºC at full charge (100% SOC), in approximate agreement with the calculated adiabatic temperature rise for the instantaneous release of the chemical potential energy ΔG.

- Flaming combustion of the cell contents ejected at failure lasts for several seconds.

- The specific heat of combustion (HOC) of the ejected cell contents at failure decreases linearly with SOC for the 18650 lithium-ion cell because of unburned nonvolatile components and incomplete combustion of volatile components.

- The specific HOC is highly dependent on cell chemistry, ranging from a low of 0.5 kJ/g for a zinc manganese dioxide (alkaline) cell to 15 kJ/g for lithium-ion cells at low SOC.

OBJECTIVE

The objective of this study was to better understand the fire hazards of individual lithium electrochemical cells that are found in passenger electronics and shipped as cargo on airplanes. To this end, methodologies were developed to measure the thermal energy released during cell failure and the combustion energy released by conflagration or explosion of the ejected cell contents.

INTRODUCTION

Failure of an electrochemical (e.g., lithium ion) cell can be triggered by a short circuit between the cathode and anode that causes internal heating or by external heating in a fire. Cell components that decompose exothermically increase the rate of self-heating, which, if sufficient, results in thermal runaway. Thermal runaway is initiated by damage to the battery (e.g., a contaminant that can build up a dendritic short), external heating of the battery, or overcharging. Thermal runaway is a term applied to internal heating caused by chemical, oxidation, or thermal decomposition reactions that result in auto-acceleration of exothermic processes and a rapid temperature rise of the system. In thermal runaway of a cell, energy is initially generated by an internal short circuit that heats the cell and causes decomposition of the cell contents in a series of exothermic reactions. This leads to the generation of decomposition products that are gaseous and are released by venting or structural failure of the battery. The gases released contain flammable components consisting of hydrocarbons, carbon monoxide, and hydrogen. In addition, solid component fragments of carbon, aluminum, and copper can be ejected. The net effect can be a rocketing cell. At the onset of thermal runaway, the energy generated from the battery exceeds its ability to dissipate the heat. Therefore, the temperature increases and causes an increase in the chemical kinetics over the heat loss. This instability causes the temperature to increase further until the reaction is completed. Once the chemical reactants are depleted, the battery achieves its final state—typically 800ºC–1000ºC. As a consequence, the efflux of gases can auto-ignite in air. Therefore, two forms of energy are released: (1) energy of decomposition, which is mainly the stored electrical energy, and (2) energy of combustion. The former usually occurs in a few seconds, whereas the latter can last up to 10 seconds.

There have been numerous studies related to the thermal runaway hazard of batteries. In particular, the development of high-energy-density lithium cells has prompted the Federal Aviation Administration to study the potential hazard of energy-storage devices shipped as cargo in airplanes. Webster [1 and 2] has produced a series of reports to document the consequences of thermal runaway with lithium batteries in shipping configurations. There have been review articles that summarize the processes (e.g., Mikolajczak et al. [3]). Detailed models that include the kinetics of the decomposition reactions and the transport of heat and electrical current have been presented [4–6]. A device that has often been used to study the energetics of electrochemical cells is the Accelerating Rate Calorimeter [7, 8], which can be used to measure the chemical kinetic rates of the cell or its components at incipient failure.

In this study, a purpose-built thermal capacitance calorimeter was used to measure the energy released during failure of electrochemical cells caused by electrical resistance heating at a constant rate. By measuring the temperature as a function of time and the heating power, the rate

of energy release due to failure of the electrochemical cell could be calculated. It was found that several kilojoules of energy were released in 1–3 seconds (i.e., the energy release rate was several kilowatts). This extremely large energy release rate was impossible to measure with the massive thermal capacitance calorimeter, so the time integral of the energy release rate (Joules of energy) was computed as a function of the state of charge (SOC) and heating rate of the calorimeter.

A separate study examined the energy released by combustion of the cell components ejected at cell failure. Typically, cell components were discharged in two separate processes that occur in rapid succession: venting of gaseous products and cell failure, with the latter contributing the bulk of the thermal and combustion energy. A peak combustion energy rate was recorded, but the total energy of combustion was deemed to be a more reliable estimate of the fire hazard of the cell.

The results of these tests, which are summarized in this report, provide a methodology for measuring the separate thermal and combustion hazards of cell failure and a basis for the quantitative assessment of cell/battery fire and explosion hazards. A similar methodology was used by Xuan Liu et al. [9] to show that the fraction of the rated electrical capacity (SOC) of an 18650 cell is directly related to combustion energy, which increases from approximately 25 kJ/cell at 0% SOC to approximately 95 kJ/cell at 80% SOC, then drops to approximately 75 kJ/cell at 100% SOC. They found that the energy of decomposition in runaway also increased with SOC from approximately 5 kJ–35 kJ over the range 0%–100% SOC. Note that the thermal capacitance calorimeter technique to measure the decomposition energy presented here is different from the adiabatic apparatus used by Walters [10]. Another study from China (University of Science and Technology of China) measured the combustion energy release rate from a lithium-ion battery in a fire calorimeter at various SOC [11].

EXPERIMENTAL

MATERIALS

The electrochemical cells tested in this study are listed by cell chemistry in table 1. Column designations describe whether they are single-use (N) or rechargeable (Y), the cell size in millimeters (e.g., 18650 is an 18 mm diameter, 65 mm long cylinder), the cell mass, the manufacturer's rating of the nominal cell potential $\varepsilon(V)$, charge capacity C (mAh), and the stored electrochemical free energy calculated from these nominal values in the appropriate units, $\Delta G_{nom} = (\varepsilon C)_{nom}$. The SOC of a rechargeable cell in this study is defined as the electrical charge stored in cell, C, divided by the nominal charge capacity, C_{nom} (i.e., SOC = (C/C_{nom})) x 100. For example, a lithium-ion cell with a nominal charge capacity of 2600 mAh (9360 Coulombs) containing 1300 mAh (4680 Coulombs) of discharge charge capacity would have an SOC = (1300 mAh/2600 mAh)(100) = 50%. The discharge capacity C never reaches the maximum discharge capacity of the cell C_{max} because 10%–15% of the charge is retained at 0% SOC to preserve the cell chemistry. By the same method of accounting, the SOC of secondary cells can be greater than 100% because $C_{max}/C_{nom} \geq 1$.

Table 1. Electrochemical cells tested in this study

MFG	Cell Chemistry	Rechargeable	Package (D*L*10)	Cell Mass (g)	Nominal Cell Potential, ε (Volts)	Nominal Charge Capacity, C (mAh)	Nominal Free Energy ΔG_{nom} (kJ/cell)
A	Lithium ion (LiCoO$_2$)	Yes	18650	44	3.7	2600	35
B	Lithium ion (LiCoO$_2$)	Yes	18650	44	3.7	2600	35
C1	Lithium ion	Yes	Pouch	23	3.7	1050	14
C2	Lithium ion	Yes	Pouch	23	3.7	1900	25
D	Nickel Metal Hydride (NiMH)	Yes	AA	26	1.2	2600	11
E	Nickel Cadmium (NiCd)	Yes	AA	21	1.2	1000	4
F	Lithium Iron Disulfide (LiFeS$_2$)	No	AA	15	1.5	3000	16
G	Lithium Manganese Dioxide (LiMnO$_2$)	No	17350	11	3.0	1500	16
H	Lithium Manganese Dioxide (LiMnO$_2$)	No	16270	16	3.0	750	8
J	Zinc Manganese Dioxide (ZnMnO$_2$)	No	11300	24	1.6	825	5

Table 2 shows typical components of a lithium-ion rechargeable cell, which is the principle focus of this study. The aluminum and copper metals are the negative and positive terminals, respectively. These metals, along with graphite and transition metal compounds (Ni/Mn/Co), are

ejected from the cell as solids, leaving the volatile organic components (SBR/PVDF/electrolyte), which range from 10%–26% of the cell mass, to burn in the fire calorimeter.

Table 2. Composition of typical lithium-ion electrochemical cell

Cell Components	Weight Percent in Cell	CAS Registry Number
Aluminum Foil	2–10	7429-90-5
Nickel Compound (proprietary)	10–25	N/A
Manganese Compound (proprietary)	6–15	N/A
Cobalt Compound (proprietary)	4–10	N/A
Styrene-Butadiene Rubber	<1	9003-55-8
Polyvinylidenefluoride (PVDF)	<5	24937-79-9
Copper Foil	2–10	7440-50-8
Carbon/Graphite	10–30	7440-44-0
Electrolyte (proprietary)	10–20	N/A
Stainless Steel and Inert Compound	Balance	N/A

METHODS

Fire Calorimetry. Individual electrochemical cells were tested in a fire (cone) calorimeter operating on the oxygen consumption principle according to a standard method [12] for measuring the combustion energy released by burning of the cell contents at failure. In these experiments, the cell was forced into failure by heating at various rates determined by the radiant power setting of the conical heater. Ignition of the ejected cell contents occurred at the hot surfaces of the heater coils. The standard ASTM E1354 sample holder [12] was modified (see figure 1) to contain the battery during the violent failure. In addition, the electric arc ignition source was removed to locate the battery surface at the standard distance of 25.4 mm from the heater. Even though the battery/cell rocketed around the sample holder after failing at a temperature of approximately 250°C, most or all of the expelled gases and solids from the cell were captured by the calorimeter.
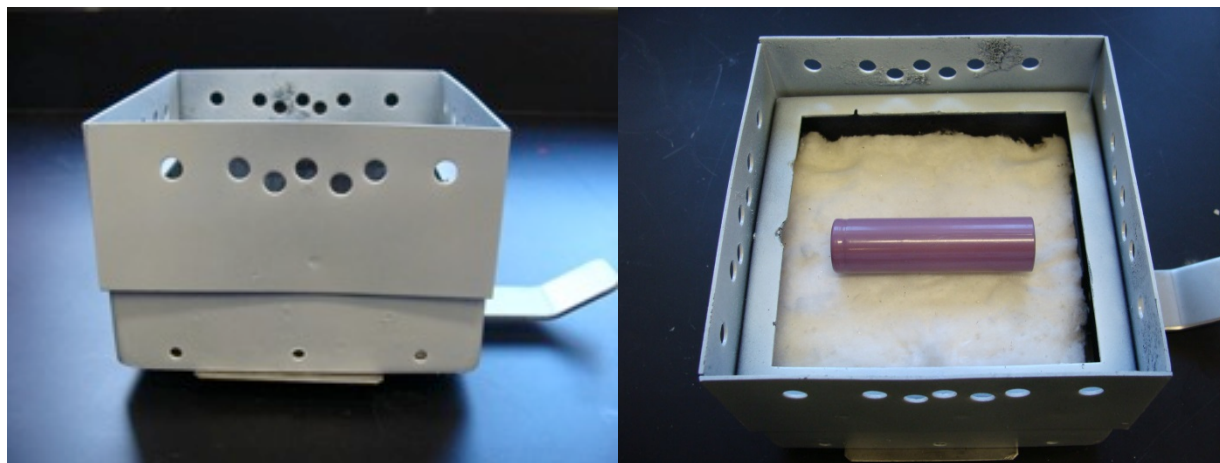
Figure 1. Modified sample holder for fire calorimeter testing of batteries

Sample Tray Modification. A modification of the standard cone sample tray was fabricated to ensure a reduction of the jet momentum of ejected battery matter and to avoid propulsion of the battery out of the fire calorimeter test space. A 25-mm-high, 1-mm-thick metal fence was attached vertically to the ASTM E1354 standard sample edge frame. The sample tray was placed against the conical heater frame so that there was no gap through which the battery could escape during the test. The battery was placed horizontally at the base of the containment tray. Figure 1 shows the modified tray holder. During a test, jetting of the battery causes it to rattle within the modified holder. A line of holes near the top allows air to enter the holder, mix with the ejected cell gases, and ignite at the heater surface. The combustion products in air are drawn into the exhaust stack of the fire calorimeter and analyzed for residual oxygen, carbon dioxide, carbon monoxide, and visible smoke. When cells are tested at high capacity (SOC), the battery contents are expelled at high velocity; it is possible that some gases escape through the holes in the sample holder without burning, which simultaneously reduces the calculated heat release and increases the measured mass loss, resulting in lower specific heats of combustion.

In these tests, the batteries listed in table 1 were exposed to radiant heat fluxes from 10–75 kW/m^2. In the case of the 3.7 V, 2600 mAh rechargeable lithium-ion battery, tests were also conducted at various fractions of the rated capacity (SOC). The time to the initial venting of gases from the battery and the time of the final vent were noted (several vents could occur). The energy-release period was very short and the normal data reduction process of the fire calorimeter was not fast enough to capture the maximum rate of energy released by combustion. Consequently, a deconvolution algorithm was used to correct the heat release rate (HRR) for the calorimeter response [13], an example of which is shown in figure 2 for the $LiCoO_2$ rechargeable cell at 70% SOC exposed to an irradiance of 50 kW/m^2. The cell begins to vent gaseous products at 89 seconds with a peak at 93 seconds. Complete failure of the cell occurs at approximately 115 seconds with a peak heat release rate (PHRR) at 120 seconds. Because the duration of these processes is comparable to the response time of the fire calorimeter, the HRRs are not well resolved, even after deconvolution. Consequently, the total heat release (THR) of the cell contents in flaming combustion, which is the time integral of the HRR (W) for both of the peaks in figure 2, is reported. Measured parameters also include the PHRR during the test, the time at which initial venting of the cell gases occurs (t_1), the time at which expulsion of the cell contents at failure (t_2) is observed, the total mass lost from the sample holder during the test, and the effective heat of combustion (HOC) based on the measured mass loss (THR/Δm) and original battery mass (THR/m_0).
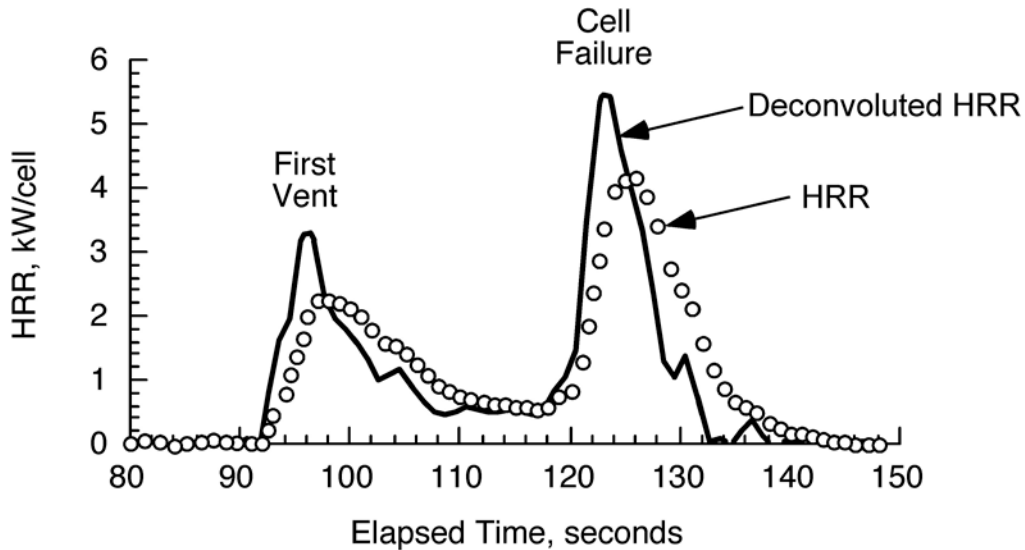
Figure 2. Lithium-ion cell failure at 70% SOC exposed to 50 kW/m^2 irradiance in fire calorimeter; points are data from standard method; solid line is data corrected for instrument response

      <u>Thermal Capacitance (Slug) Calorimeter.</u> A thermal capacitance calorimeter, shown in figure 3, was designed and fabricated to measure the thermal energy associated with cell failure. The calorimetric method consisted of the following operations: (1) a single cell was heated to failure by wrapping it with a nickel-chromium (Nichrome) resistance heating wire whose voltage (V) and current (I) were measured to provide the electrical power (P = VI) delivered to the cell; (2) the assembly was continuously weighed and recorded; and (3) the temperature on the outer steel jacket of the calorimeter was also measured and recorded over time. Occasionally, the cell temperature was also measured.
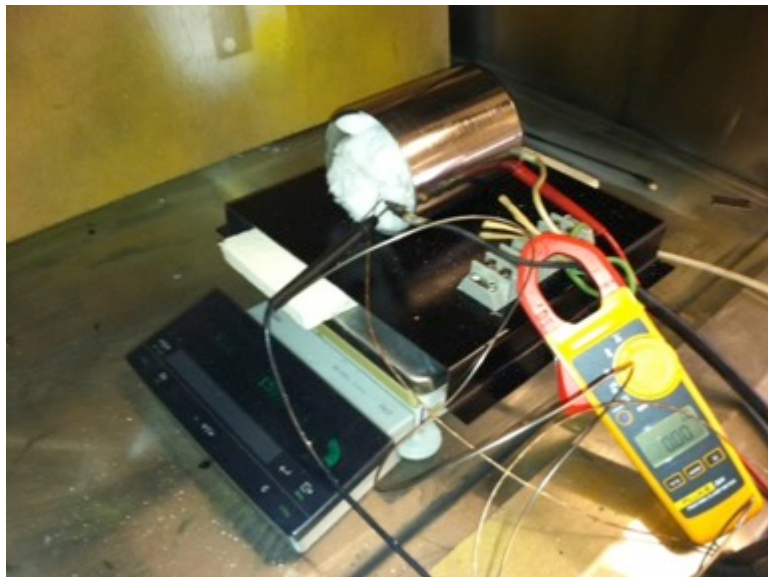
Figure 3. Experiment in thermal capacitance calorimeter

The thermal capacitance calorimeter consists of the following components, as shown in figure 4:

- Electrochemical cell (single-cell battery) in a close-fitting copper cylindrical sleeve.
- Ceramic paper wrapped around copper sleeve for electrical insulation.
- Nickel-chromium resistance heating wire wrapped around ceramic paper/copper sleeve to heat the electrochemical cell to failure.
- Ceramic wool wrapped around the heating cell to thermally insulate it from the environment.
- Entire assembly jacketed by thin-walled stainless steel cylinder 76 mm (3 inches) in diameter for handling purposes.
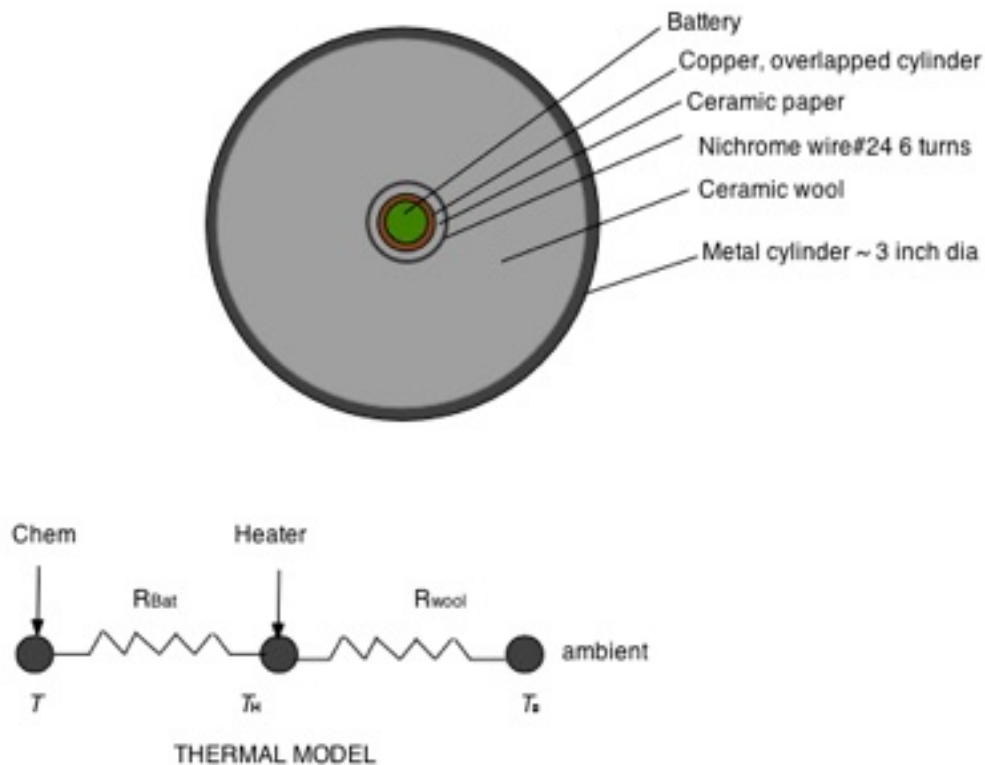
Figure 4. Schematic drawing of thermal capacitance calorimeter

MODEL FOR ANALYSIS. Energy developed by electrochemical cell at failure in addition to electrical resistance heating is determined by computing the input power; the internal energy of the copper cylinder and battery; heat loss to the surroundings (electric heater wires and ceramic blanket insulation); and enthalpy expelled as heated mass (cell contents).

In the analysis, the following assumptions are made:

- The battery and copper cylinder are considered thermally thin.
- The heat loss is by conduction into a semi-infinite media.
- The heat loss is calibrated by matching the heat capacity of a battery-equivalent aluminum cylinder.
- Total energies are computed from the data by evaluating a time integral of the conservation of mass and energy for the battery.
- The specific heat of the battery is computed as 0.95 +/- 0.03 J/g-K.

These assumptions are reasonable and can be justified by heat transfer. The specific heat of the battery is needed in the analysis; that has been derived by experiment after calibration with a cylinder of aluminum in which the specific heat is known (see appendix B). An energy balance on the calorimeter system shown in figure 4 results in the following equation for the rate of energy release during cell failure:

$$\dot{Q}_b = c_b \frac{d(mT)}{dt} + \dot{Q}_{loss} - P - c_g T \frac{dm}{dt} \tag{1}$$

In equation 1, $\beta = 1.4$ $W\text{-}s^{1/2}/K$ is found by calibration with an aluminum solid cylinder for a linear surface temperature rise into semi-infinite media of ceramic insulation and copper wire connectors; the rate of heat loss is:

$$\dot{Q}_{loss} = \beta \frac{T - T_i}{\sqrt{t}} \tag{2}$$

Because of the rapid changes in temperature and mass, it is difficult to accurately compute the derivatives so that equation 1 is integrated to obtain the energy release at time, t:

$$Q_b(t) = \int_0^t \dot{Q}_b(x)\,dx = (mc)_{Cu}(T - T_i) + c_b(mT - m_i T_i) + \int_0^t \dot{Q}_{loss}(x)\,dx - Pt - c_g \int_{m_i}^{m} T(y)\,dy \tag{3}$$

The values determined for the constants in equation 3 are: $(mc)_{Cu} = 8.4$ J/K, $c_b = 0.95$ J/g-K, and $c_g 1.05$ J/g-K. A typical result showing the magnitude of each of the terms in equation 3 is shown in figure 5. Failure of the cell occurs at approximately 600 seconds into the test, at which point the decomposition energy first increases to approximately 5 kJ and the first venting of gaseous cell contents occurs. This is relatively mild, approximately 4 g abruptly, then there is a slow loss of another 4 g to approximately 650 seconds, at which time the major event occurs (thermal runaway) with an abrupt drop by 12 g more (out of 44 g initially). The energy increases to approximately 28 kJ, and the temperature increases from approximately 250°C to 800°C in approximately 2 seconds. The integration of the exhaust material is significant; therefore, the assumption of $c_g = 1.05$ J/g-K is problematic because some solids make up this efflux, and this value does not reflect an increase due to temperature. A higher value would increase the

computed decomposition energy. For example, a specific heat of 1.2 J/g-K for the efflux mixture, indicative of temperature effect on the gas mixture, would raise the jump value from 28 to 30 kJ/g.
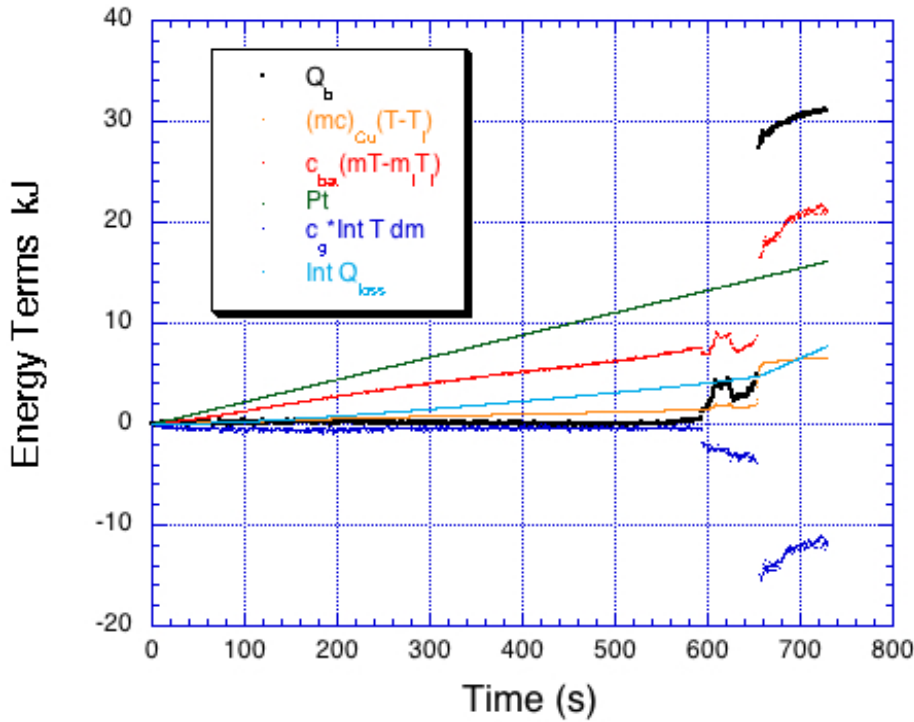

Figure 5. Energy terms for test 29, SOC = 80%, P = 22.1 W

RESULTS AND DISCUSSION

COMBUSTION ENERGY

The results from the fire calorimeter tests for the rechargeable (secondary) cells listed in table 1 are given in tables 3 and 4. Fire calorimeter results for the non-rechargeable (primary) cells are given in table 5. Each cell type is different, with the combustion energy ranging from approximately 1–4 kJ/g of original battery. The radiant power of the various heat fluxes changed the time to venting (t_1) and failure (t_2) but not the total energy released in flaming combustion (THR) to any great extent. The SOC had the most influence on the combustion energy as shown for cell A. The combustion energy per original mass decreased from approximately 2 to 1.5 kJ/g as SOC increased from 20% to 100%. This decrease in combustion energy may be due to the combustible gases being ejected beyond the hood of the cone calorimeter and therefore were not measured.

The effective HOC of the cell contents, HOC = THR/Δm, ranged from approximately 2–25 kJ/g and had a tendency to increase slightly with the radiant heating level. The result shows the differences among the batteries.

9

Table 3. Fire calorimeter data for 18650 lithium-ion rechargeable (secondary) cells

| Cell	Chemistry	SOC (%)	Heat Flux (kW/m^2)	t_1 (s)	t_2 (s)	Peak HRR (kW)	THR (kJ)	Mass Loss, Δm (g)	HOC (kJ/g)	THR/m_0 (kJ/g)
A	LiCoO$_2$	100	10	731	n/a	0.2	9	4	2.2	0.2
A	LiCoO$_2$	100	30	165	242	13.7	84	10.3	8.2	1.9
A	LiCoO$_2$	100	30	166	242	9.8	76	12.6	6.0	1.7
A	LiCoO$_2$	100	50	109	159	10.2	100	10.1	9.9	2.3
A	LiCoO$_2$	100	50	96	137	16.2	93	9.6	9.7	2.1
A	LiCoO$_2$	100	75	56	75	12.3	82	9.1	9.0	1.9
A	LiCoO$_2$	100	75	50	71	16.2	93	9.1	10.2	2.1
A	LiCoO$_2$	20	50	86	n/a	4.4	59	6	9.7	1.3
A	LiCoO$_2$	20	50	86	n/a	2.5	102	6.5	15.6	2.2
A	LiCoO$_2$	20	50	87	n/a	3.3	92	6.1	15.0	2.0
A	LiCoO$_2$	20	50	93	n/a	3.0	97	6.3	15.5	2.1
A	LiCoO$_2$	20	50	86	n/a	3.5	81	6.3	12.8	1.8
A	LiCoO$_2$	30	50	102	130	6.0	92	5.9	15.6	2.0
A	LiCoO$_2$	30	50	104	132	4.0	95	5.7	16.8	2.1
A	LiCoO$_2$	30	50	102	133	3.2	86	5.3	16.1	1.9
A	LiCoO$_2$	30	50	86	130	2.7	84	5.7	14.8	1.9
A	LiCoO$_2$	30	50	92	125	9.2	78	8.1	9.6	1.7
A	LiCoO$_2$	50	50	100	135	7.4	73	n/a	—	1.6
A	LiCoO$_2$	50	50	106	123	7.4	68	7.6	9.0	1.5
A	LiCoO$_2$	50	50	95	132	10.4	93	n/a	—	2.0
A	LiCoO$_2$	50	50	99	126	9.2	83	6.9	12.1	1.8
A	LiCoO$_2$	70	50	93	122	5.4	64	22.4	2.8	1.4
A	LiCoO$_2$	70	50	93	120	6.7	70	12	5.8	1.5
A	LiCoO$_2$	70	50	102	129	5.3	63	14	4.5	1.4
A	LiCoO$_2$	70	50	102	124	8.4	77	11.8	6.5	1.7
A	LiCoO$_2$	70	50	93	121	7.2	69	10.6	6.5	1.5
A	LiCoO$_2$	100	50	86	112	6.2	58	13.3	4.4	1.3
A	LiCoO$_2$	100	50	92	112	3.3	68	20.8	3.3	1.5
A	LiCoO$_2$	100	50	103	117	12.1	59	n/a	—	1.3
A	LiCoO$_2$	100	50	93	119	5.9	57	13.7	4.2	1.3
A	LiCoO$_2$	100	50	88	113	8.4	62	12.3	5.1	1.4
B	LiCoO$_2$	100	50	86		4.2	48	4.1	11.7	2.4
B	LiCoO$_2$	100	50	61		5.6	55	5	11.0	2.7

Table 4. Fire calorimeter data for lithium-ion, NiMH, and NiCd rechargeable (secondary) cells

Cell	Chemistry	SOC (%)	Heat Flux (kW/m²)	t_1 (s)	t_2 (s)	Peak HRR (kW)	THR (kJ)	Mass Loss, Δm (g)	HOC (kJ/g)	THR/m_0 (kJ/g)
C1	Li-ion	50	10	500	N/A	0.2	6	5.2	1.2	0.3
C1	Li-ion	50	30	112	N/A	9.2	57	3.3	17.3	2.4
C1	Li-ion	50	30	130	N/A	8.9	47	2.9	16.2	2.0
C1	Li-ion	50	50	38	51	6.0	77	5.1	15.1	3.3
C1	Li-ion	50	50	48	63	5.7	75	5.6	13.4	3.2
C1	Li-ion	50	75	14	44	7.1	109	6.1	17.9	4.7
C1	Li-ion	50	75	22	31	5.8	97	7.2	13.5	4.2
C2	Li-ion	50	10	512	N/A	0.5	0	4.3	0	0.0
C2	Li-ion	50	30	64	84	7.8	156	10.2	15.3	3.8
C2	Li-ion	50	30	68	88	7.0	145	9.8	14.8	3.5
C2	Li-ion	50	50	35	52	8.0	162	11.1	14.6	3.9
C2	Li-ion	50	50	35	58	5.8	147	11.1	13.2	3.6
C2	Li-ion	50	75	19	35	8.9	165	12.1	13.6	4.0
C2	Li-ion	50	75	22	39	7.4	170	12	14.2	4.1
D	NiMH	100	50	212	357	0.0	0	2.6	0	0.0
D	NiMH	100	50	353	N/A	0.7	13	1.1	11.8	0.5
E	NiCd	100	50	N/A	N/A	0	0	6.5	0	0.0
E	NiCd	100	50	N/A	N/A	0	0	5.8	0	0.0

**Table 5. Fire calorimeter data for non-rechargeable (primary) cells**

Cell	Chemistry	SOC (%)	Heat Flux (kW/m²)	t_1 (s)	t_2 (s)	Peak HRR (kW)	THR (kJ)	Mass Loss, Δm (g)	HOC (kJ/g)	THR/m_0 (kJ/g)
F	$LiFeS_2$	100	50	80	160	3	51	2	25.5	3.5
G	$LiMnO_2$	100	30	104	149	4.2	42	4.7	8.9	2.6
G	$LiMnO_2$	100	30	113	149	3.6	55	8.4	6.5	3.4
G	$LiMnO_2$	100	50	74	94	3.9	52	4.4	11.9	3.2
G	$LiMnO_2$	100	50	69	89	4.7	74	4.4	16.7	4.5
G	$LiMnO_2$	100	75	48	68	5.9	64	3.8	16.8	3.9
G	$LiMnO_2$	100	75	52	67	3.5	45	4.3	10.4	2.7
H	$LiMnO_2$	100	30	115	148	2.8	27	3.3	8.2	2.5
H	$LiMnO_2$	100	30	118	161	3.1	32	3.2	10	3
H	$LiMnO_2$	100	50	77	85	3.9	20	3.4	6	1.9
H	$LiMnO_2$	100	50	90	118	3.7	33	3.5	9.5	3.2
H	$LiMnO_2$	100	75	54	65	6.5	34	2.3	14.6	3.2
H	$LiMnO_2$	100	75	54	70	4.2	31	3.7	8.5	2.9
J	$ZnMnO_2$	100	50	204		0.6	17	2.7	6.3	0.7
J	$ZnMnO_2$	100	50	202		0.6	10	3.0	3.3	0.4

Figure 6 shows the PHRR and effective HOC of the cell contents vs. SOC for cell A at an external heat flux of 50 kW/m^2 from table 3. The PHRR increases monotonically with SOC, but the HOC of the ejected material decreases from approximately 15 to 5 kJ/g over the same range.
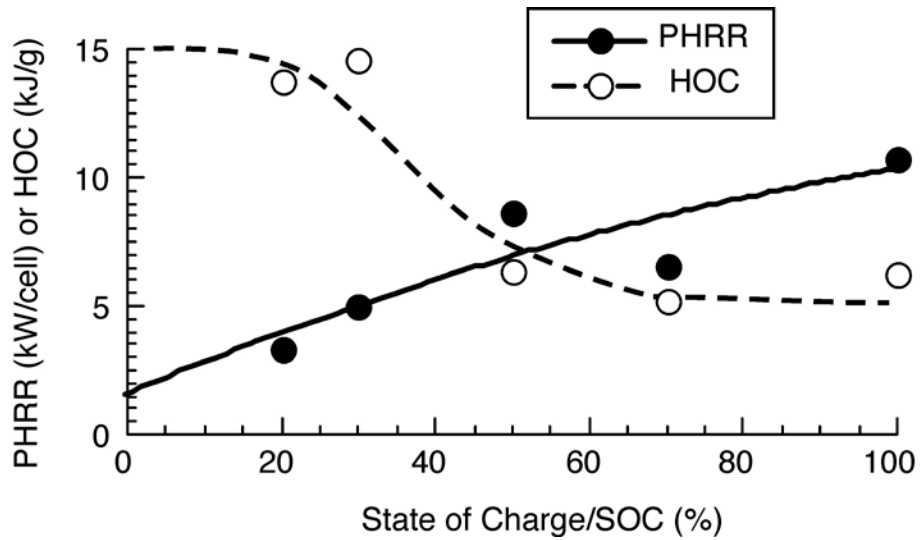

**Figure 6. The HOC and PHRR vs. SOC for a lithium-ion 18650 (cell A)
at a heat flux of 50 kW/m^2**

Figure 7 shows the ratio of the carbon dioxide yield to the carbon monoxide yield (i.e., kg-CO$_x$/Δm) for the same fire calorimeter data that are plotted in figure 6. The monotonic decrease in the CO$_2$/CO mass ratio during conflagration of the cell components suggests that transition metals or halogens ejected at high SOC may be inhibiting combustion, as evidenced by the decreased oxidation of CO to CO$_2$ in the flame.
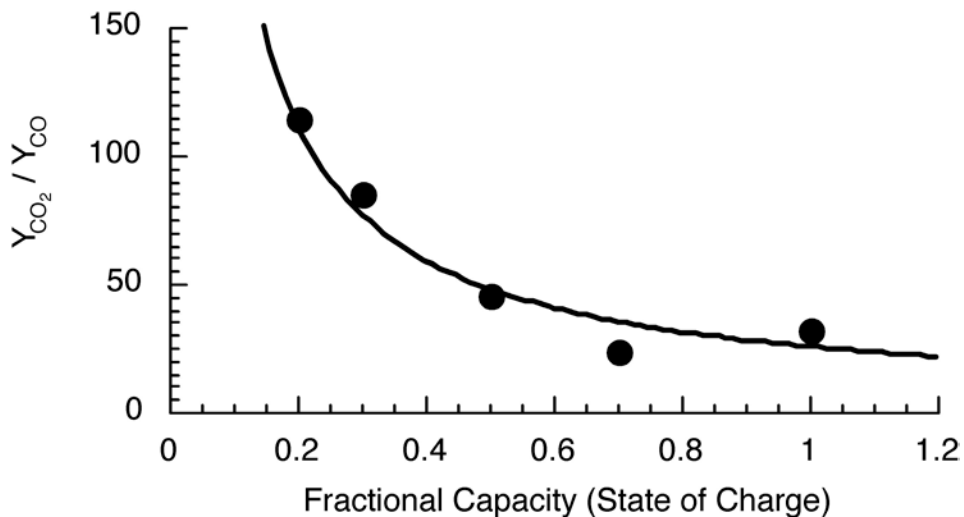
**Figure 7. Ratio of CO$_2$ yield to CO yield vs. SOC for lithium-ion cell A at 50 kW/m^2 radiant
flux: each point is an average of 4 tests**

A more complete presentation of the effect of the SOC on the combustion energy and mass loss is shown in figure 8. Conversely, the effective HOC of cell A increases within the heating rate, as shown in figure 9. Also shown are the energy and mass loss associated with the HOC.
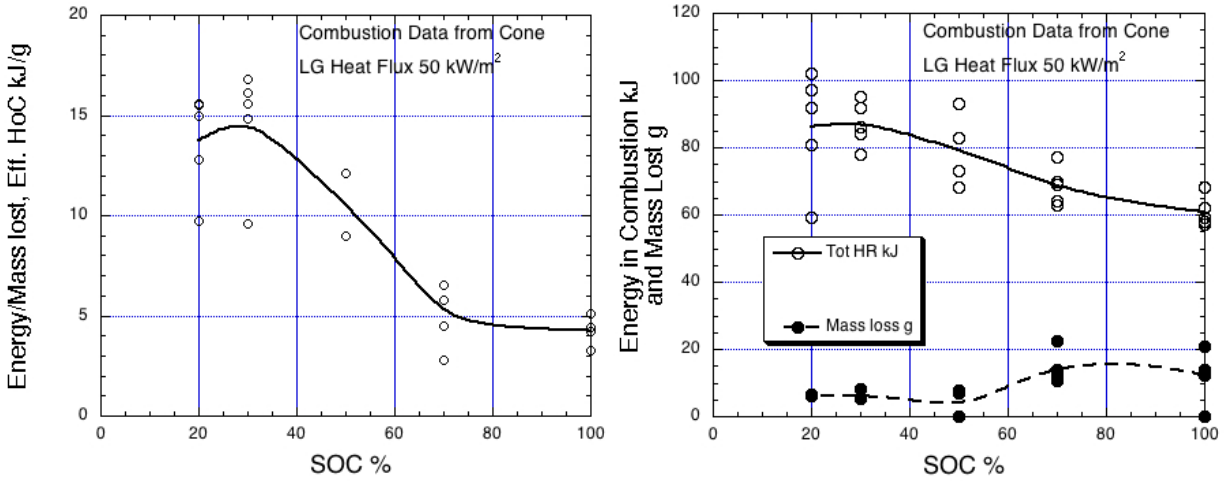
Figure 8. Energy of combustion (THR), mass loss (Δm), and effective HOC vs. SOC for the lithium-ion 18650 cell A at an external heat flux of 50 kW/m^2
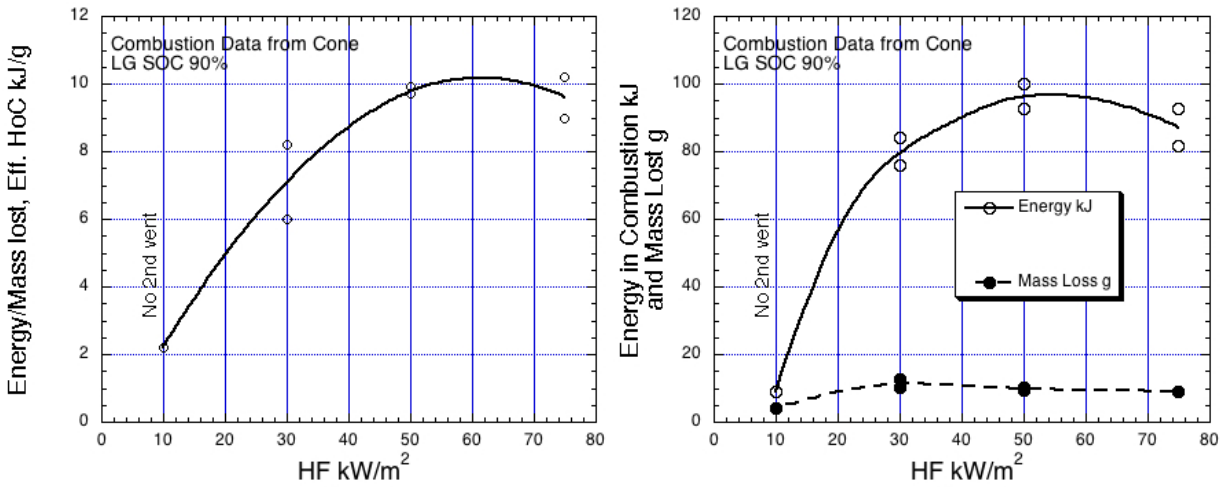
Figure 9. Combustion energy (THR), mass loss (Δm), and effective HOC vs. external heat flux in the fire calorimeter for lithium-ion 18650 cell A

The HOC is a significant fire parameter because it can be related to the lower flammability limit (LFL) of the gases. Assuming the ejected mass is primarily a gaseous species, the LFL can be approximately computed in molar units as:

$$LFL = c_p(1300°C-T)/HOC \qquad (4)$$

where T is the temperature of the exiting gases [14].

For example, for cell A in figures 6 and 8, the effective HOC can vary from approximately

HOC = 5–15 kJ/g. If the unburned gases are emitted at the temperature of cell failure (250ºC) and it is assumed that the molecular weight of the mixture is based on a mixture of hydrogen, methane, carbon monoxide, and hydrocarbon fragments taken as approximately 30 g/mol, the LFL, expressed as a volume fraction of fuel in air (v/v), is

$$LFL = (0.03 \text{ kJ/mol})(1300°C–250°C)/[(15 \text{ to } 5 \text{ kJ/g})(30 \text{ g/mol})] = 0.07 \text{ to } 0.21 \text{ v/v} \qquad (5)$$

These LFLs are high for gases in general, which typically are approximately 0.05 v/v for hydrocarbons, which is further indication of flame inhibition by lithium-ion cell components at high SOC. This number would drop because some of the ejected material is solid and, therefore, the HOC of the gases would have a higher value if these solids did not burn. In addition, if the battery heat is decomposing its packaging materials or other surrounding materials, the HOC of all the gases would tend to increase and the LFL would drop. In general, to get an "explosive" mixture from this battery alone, it appears its ejected gases would have a relatively high LFL and would need a significant release of unburned material to reach this concentration. This is consistent with a study at the FAA [15] where the LFL was calculated using LeChatlier's mixing rule from the quantitative analysis of gases sampled using a GC.

ELECTROCHEMICAL ENERGY

The electrochemical energy released as heat during the failure of the 18650 lithium-ion cell B in the thermal capacitance calorimeter was measured as a function of the heater power and the SOC of the battery. The results of these tests are given in table 6. A typical test produced data and results as indicated by Test 27 at 80% SOC and an electrical resistance heating of approximately 10 W, as shown in figure 10. The first venting of cell B occurred at t_1 = 1380s. The second vent occurred at t_2 = 1520s and was accompanied by a temperature rise from approximately 230ºC–770ºC in a matter of seconds. The computed energy release (exotherm) is approximately 27 kJ plus approximately 3 kJ from the first vent. The first venting may lead to conflagration of the vented gases either with or without a pilot ignition source, but an intermittent electric arc was used in these measurements to force ignition. Therefore, at least three sources of energy result from failure of the cell: (1) the electrochemical energy released by a short circuit in the cell, (2) the energy released by thermal decomposition of the cell components, and (3) the energy associated with the burning of the ejected cell components. The kinetic energy of the ejected hot solid particles is expected to be relatively small.
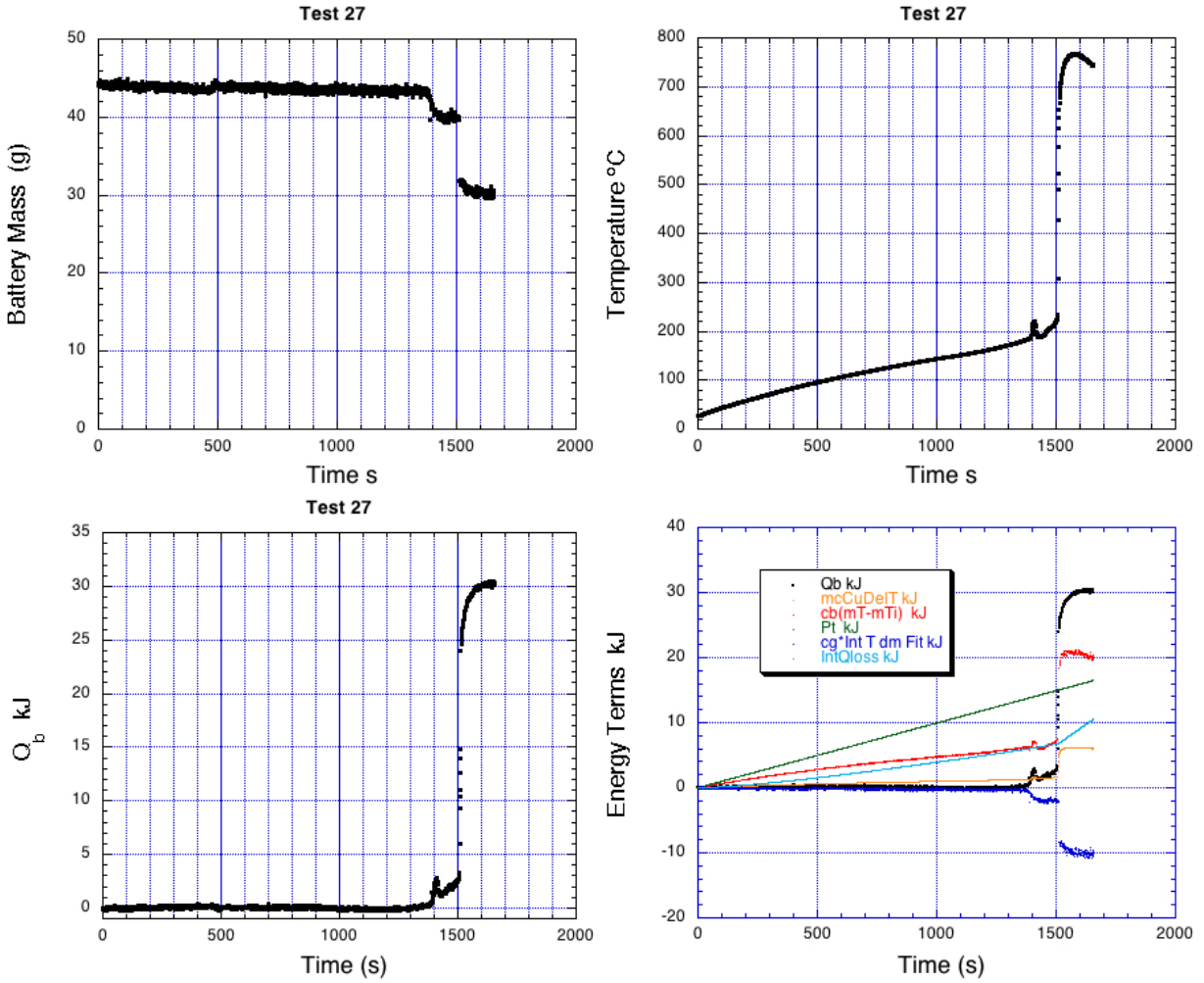
Figure 10. Test results in decomposition of battery at 80% SOC and *P* = 9.95 W

Table 6. Results of 18650 lithium-ion cell B tests in the thermal capacitance calorimeter

Test No	SOC %	P (W)	m_0, g	t_1, s	m_1, g	t_2, s	m_2, g	Final Mass g	T_1, ºC	T_2, ºC	T_{max} ºC	Q_b, kJ
9	0.5V	25.3	44.3	400	44	400	34	38.6	190	230	800	2
19	0	26.9	44	400	42	800	37	na	180	280	560	0
18	22	27.6	43.8	450	41	550	34	38.2	200	270	670	17
16	30	23.6	43.8	630	41	700	37	38.2	200	260	580	17
14	40	26.1	44.2	540	42	630	37	37.9	210	270	650	21
21	60	25.7	44	400	41	560	31	35.7	180	240	740	28
13	60	26.4	44.3	500	40	580	31	33.9	200	250	950	25
27	80	9.95	44.2	1380	40	1520	30	32.6	n/a	230	770	30
29	80	22.1	44.1	590	43	670	28	32.9	n/a	270	800	31
11	80	23.6	44.1	550	42	640	32	31.9	190	250	910	33
7	80	25.2	44.3	570	43	640	32	32.4	200	250	1350	40
8	80	25.2	44.2	440	40	540	29	31.7	200	250	840	33
30	80	36.4	44	350	40	395	31	30.6	n/a	260	830	32
31	80	49.5	44.2	220	38	270	28	32.8	n/a	270	870	33
32	80	58.8	44.1	174	40	220	31	32.1	n/a	280	820	28
33	80	73.2	44	130	41	165	25	30	n/a	n/a	n/a	n/a
34	80	74.2	44.1	125	40	165	29	32	n/a	270	930	35
23	90	27	44.1	500	42	550	25	25.9	200	240	640	20
15	100	25	44.3	520	41	570	29	27.5	200	250	800	31
12	100	25.5	44.3	540	41	600	n/a	29	n/a	n/a	1200	48
17	100	25.6	44.1	500	40	550	24	24.6	200	250	800	30
10	100	25.8	44.1	480	40	540	-4	21.9	190	250	n/a	n/a

In general, the results for all the tests were insensitive to the power input, as shown in figures 11–13. The temperatures at the onset of runaway were approximately 260ºC and afterwards were approximately 830ºC. Mass loss at the first venting is approximately 3 g and at runaway is approximately 10–12 g, on average. The energy release is approximately 33 +/- 3 kJ and occurs within 5 seconds or less.
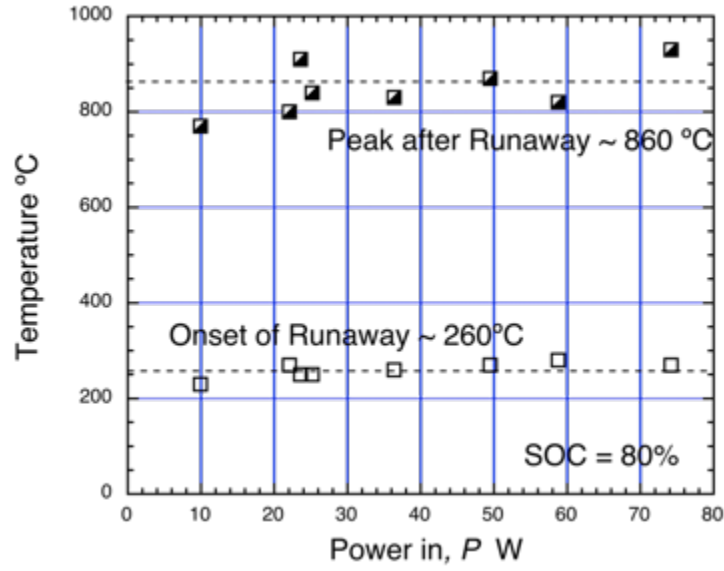
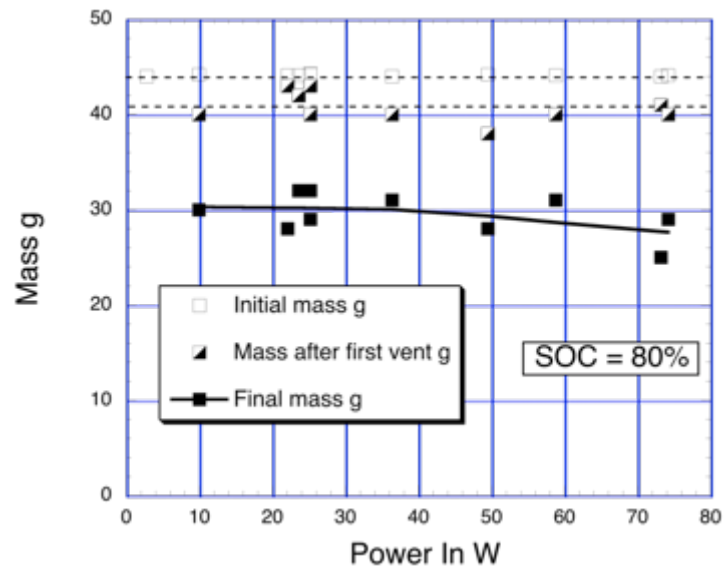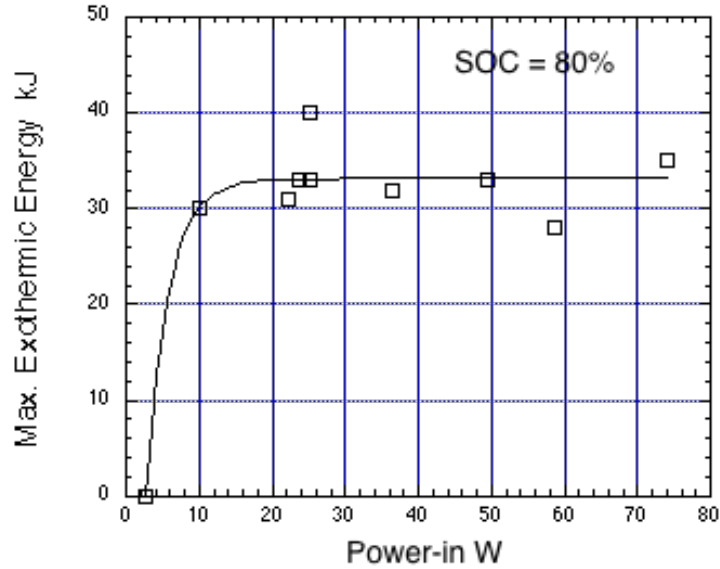**Figure 11. Critical temperatures for lithium-ion 18650 cell B at 80% SOC**

Figure 12. Initial mass (m_0), mass at after first vent (m_1), mass at the onset of failure (m_2), and final mass (m_{final}) after thermal runaway

Figure 13. Maximum energy released Q_b vs. input power for 18650 lithium-ion cell B at 80% SOC

However, the SOC affected these results, as shown in figures 14–16. Temperature increases at failure from approximately 560ºC at 0% SOC to over 1000ºC at 100% SOC. Here, the input power was fixed at approximately 26 W. The increase in temperature at 0% SOC is due to the input power and not the activity of the battery. It should be noted that 0% SOC of charge does not mean zero capacity for the cell. The residual capacity is approximately 10%–15% of the rated capacity (see table 1) at 0% SOC. A test at 0.5 V (Test 9) indicated results similar to that of 0% SOC. In both tests at this low level, there was venting from the battery. The exothermic energy output was measured to increase from approximately 0 or 2 to approximately 40 +/-8 kJ at 100%.
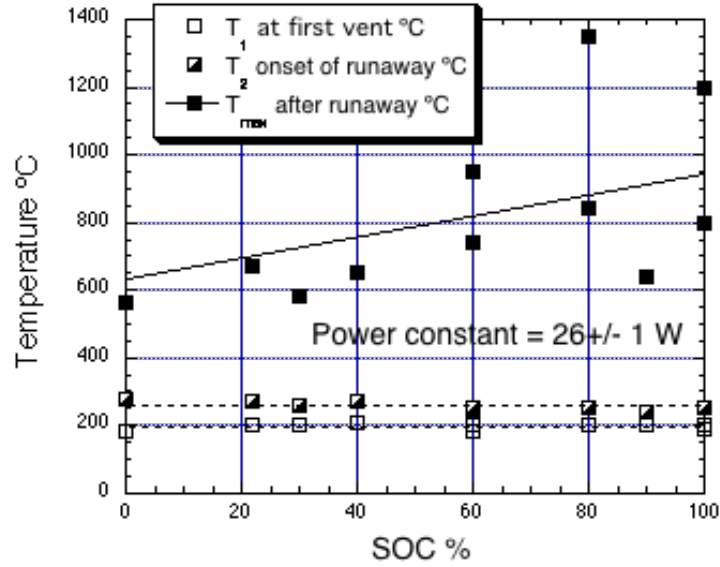
Figure 14. Critical temperatures vs. SOC for 18650 lithium-ion cell B at 26 W heater input power
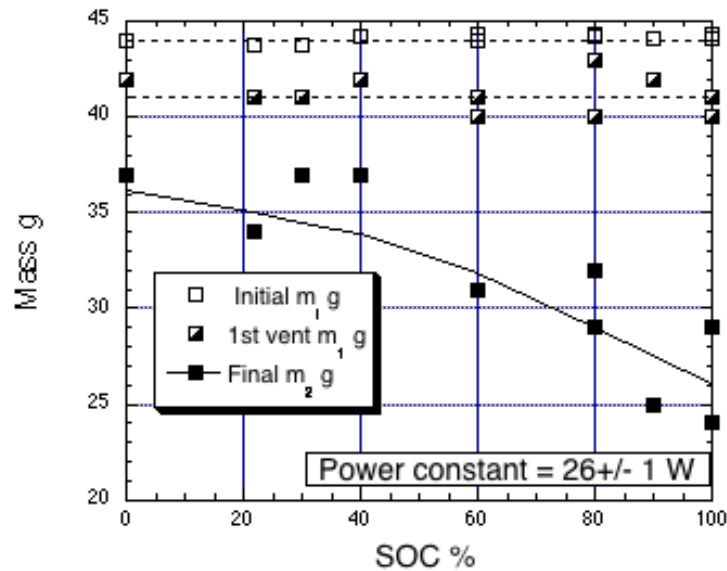
Figure 15. Initial mass m_0, mass after first vent m_1, and final mass after failure m_2 for 18650 lithium-ion cell B at 26 W heater input power
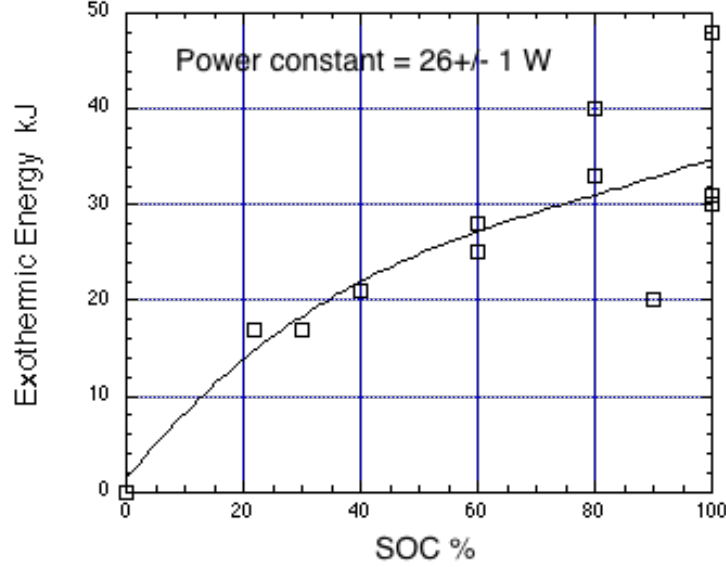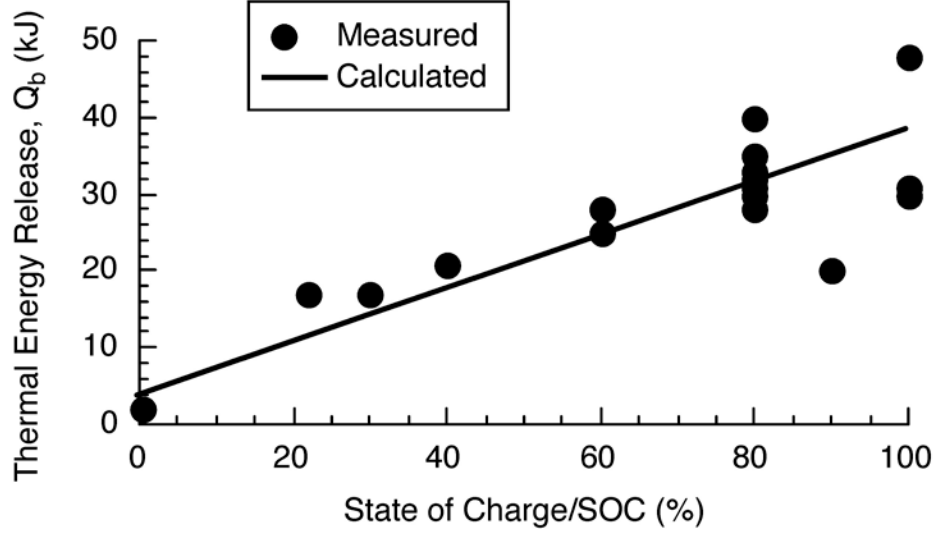
Figure 16. Maximum energy released Q_b vs. SOC for 18650 lithium-ion cell B at 26 W heater input power

As shown in figures 13–15, the SOC was a significant independent variable. The temperature after failure T_{max}, the mass lost Δm, and the final decomposition energy Q_b all increased with the SOC.

The strong dependence of the temperature rise, ejected mass, and energy release at cell failure on SOC shown in figures 14–16 is related to the stored electrochemical free energy, $\Delta G = \varepsilon C$, where ε is the cell potential in volts and C is the electrical charge in Coulombs (A-s). It is conventional in lithium-ion rechargeable cells to retain approximately 10%–15% of the nominal charge capacity at 0% SOC to preserve the cell chemistry. Because ε is relatively independent of C, the electrochemical free energy of a lithium-ion cell is related to the SOC:

$$\Delta G = 0.1(\varepsilon C)_{nom} + \frac{\text{SOC}(\%)}{100}(\varepsilon C)_{nom} = \left(0.1 + \frac{\text{SOC}(\%)}{100}\right)(\varepsilon C)_{nom} \tag{6}$$

If the energy released at cell failure in the thermal capacitance calorimeter (see figure 16) is the electrochemical free energy at a particular SOC, then $Q_b \approx \Delta G$. Figure 17 is a plot of Q_b from figure 16 vs. SOC. Also plotted as a solid line in figure 17 is ΔG of equation 6 for a nominal energy at 100% SOC, $(\varepsilon C)_{nom} = (3.7\text{V})(2.6 \text{ Ah})(3600 \text{ seconds/hour}) = 34.63$ kJ from table 1. The agreement between the measured (Q_b) and calculated (ΔG) energy release at cell failure is well within the experimental error of the thermal capacitance calorimeter measurements.

Figure 17. Measured (Q_b) and calculated (ΔG) thermal energy released at failure vs. SOC for the 18650 lithium-ion cell

The maximum temperature of the lithium-ion cell at failure should also be calculable from ΔG if the energy release during the 2-s failure event produces an adiabatic temperature rise. In this case, the energy release per cell is $Q_b = m_0 c_b (T_{max} - T_2)$. Using $m_0 = 45g$ from table 1, $T_2 = 260°C$ from table 6, and the measured heat capacity of the cell, $c_b = 0.95$ J/g-K, the computed temperature rise at failure is:

$$T_{max} = T_2 + \frac{Q_b}{c_b m_0} = 260°C + \frac{Q_b}{(0.95\,J/gK)(45g/cell)} \tag{7}$$

Figure 18 is a plot of the measured T_{max} in figure 14 vs. SOC along with the adiabatic T_{max} calculated from the measured Q_b and the nominal ΔG (equation 6).In figure 18 the solid circles are measured values. Open circles are Adiabatic Values Calculated From Measured Energy Release, Q_b. The Solid line is Adiabatic Calculation Using Electrochemical Free Energy, ΔG. The close agreement between measured T_{max} and the values calculated from Q_b suggests that the assumption of an adiabatic temperature rise is appropriate. The agreement between measured T_{max} and the values computed using ΔG of equation 6 is probably within the experimental error of the measurements, though the measured T_{max} at 0% SOC appears to be significantly higher than the theoretical value, suggesting an additional source of chemical energy (e.g., thermal decomposition of the cell components).
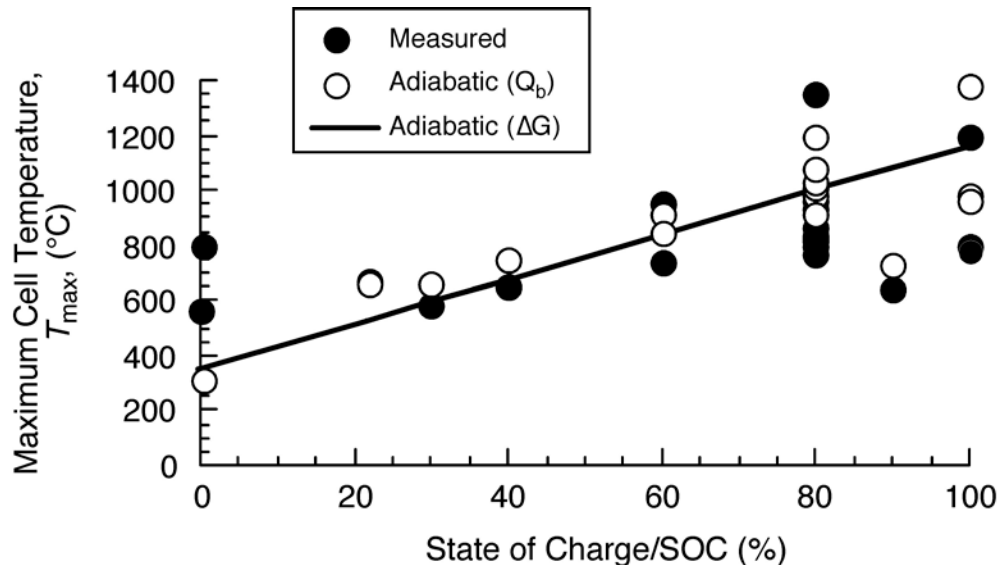
Figure 18. Maximum surface temperatures of 18650 lithium-ion cell at failure vs. SOC

CONCLUSIONS

The primary hazards associated with the failure of an individual electrochemical cell are the high surface temperature (1000ºC) caused by rapid release of chemical energy of the cell contents at failure and subsequent conflagration or explosion of the ejected cell contents. Both the hot cell and the flaming gases can ignite adjacent combustible materials or trigger failure in adjacent cells. Representative energetic characteristics of an 18650 lithium-ion cell heated to failure are:

• Chemical energy released as heat at failure is rapid ($\approx$ 2s) and raises the cell temperature adiabatically to as much as 1000°C at high states of charge (SOC).

• The chemical energy release at failure increases from approximately 2 kJ/cell at 0% SOC to 40 kJ/cell at 100% SOC and approximates the chemical free energy, Δ = Voltage x Charge.

• Conflagration (burning) of the cell contents ejected at failure lasts for approximately 10 seconds.

• The energy released by burning of the cell contents in a diffusion flame (combustion energy) is usually greater than the chemical energy of the cell contents released as heat at failure (thermal energy).

• Combustion energy (kJ) and the specific heat of combustion of the cell contents (kJ/g) decrease with SOC because of incomplete burning. This trend is the result of a higher proportion of nonvolatile components and combustion inhibition of the ejected cell contents at high SOC.

22

REFERENCES

1. Webster, H., "Flammability Assessment of Bulk-Packed, Rechargeable Lithium-Ion Cells in Transport Category Aircraft," DOT/FAA/AR-06/38, Office of Aviation Research and Development, September 2006.

2. Webster, H., "Fire Protection for the Shipment of Lithium Batteries in Aircraft Cargo Compartments," DOT/FAA/AR-10/31, November 2010.

3. Mikolajczak, C., Kahn, M., White, K., and Long, R.T., "Lithium-Ion Batteries Hazard and Use Assessment," The Fire Protection Research Foundation, July 2011.

4. Doughty, D. H., Butler, P.C., Jungst, R. G., and Roth, E.P., "Lithium Battery Thermal Models," *Journal of Power Sources*, Vol. 110, 2002, pp. 357–363.

5. Spotnitz, R., and Franklin, J., "Abuse Behavior of High-Power, Lithium-Ion Cells, *Journal of Power Sources,* Vol. 113, 2003, pp. 81–100.

6. Wang, Q., Ping, P., and Sun, J., "Catastrophe Analysis of Cylindrical Lithium Ion Battery," *Nonlinear Dynamics,* 2010, Vol. 61, pp. 763–772.

7. Roth, E.P. and Doughty, D.H., "Thermal Abuse of High-Power 18650 Li-Ion Cells," *Journal of Power Sources*, Vol. 128, 2004, pp. 308–318.

8. Spotnitz, R.M., Weaver, J., Yeduvaka, G., Dougthty, D.H., and Roth, E.P., "Simulation of Abuse Tolerance of Lithium-Ion Battery Packs, *Journal of Power Sources*, Vol. 163, 2007, pp. 1080–1086.

9. Liu, X., Stoliarov, S.I., Denlinger, M., Masias, A. and Snyder, K. "Comprehensive Calorimetry of the Thermally-Induced Failure of a Lithium Ion Battery," *Fire and Materials Conference*, San Francisco, California, February 2015.

10. Walters, R. and Lyon, R., "Energy Release From Li-Ion Batteries in the Oxygen Bomb," *Fire and Materials Conference*, San Francisco, California, February 2015.

11. Fu, Y., Song, L., Kaiyuan, L., et al., "An Experimental Study on Burning Behaviors of 18650 Lithium Ion
    Batteries Using a Cone Calorimeter," *Journal of Power Sources*, Vol. 273, 2015, pp. 216–222.

12. ASTM Standard E 7354-04a, "Standard Test Method for Heat and Visible Smoke Release Rates for Materials and Products Using an Oxygen Consumption Calorimeter," ASTM International, West Conshohocken, Pennsylvania, 2007.

13. Filipczak, R., Crowley, S., and Lyon, R.E., "Heat Release Rate Measurements of Thin Samples in the OSU Apparatus and the Cone Calorimeter," *Fire Safety Journal*, Vol. 40, No. 7, 2005, pp. 628–645.

14. Quintiere, J. G., *Fundamentals of Fire Phenomena,* John Wiley and Sons, Ltd*.,* 2006, p. 104.

15. Maloney, T., "Lithium Battery Thermal Runaway Vent Gas Analysis," DOT/FAA/TC-15/59, in press.

APPENDIX A. DECONVOLUTION MODEL

When fire tests are conducted and data are collected vs. time, the recorded signal is always a distorted version of what is actually occurring in the test (i.e., the event history). This distortion has two components: (1) the time delay between the event and the recording device, and (2) distortion or smearing of the recorded signal due to mixing of gases (fire tests), response time of sensors (cone calorimeter), or thermal inertia of the Ohio State University (OSU) fire test apparatus. The time delay is corrected by subtracting the transit time of the signal between the event and the recording device from the recorded time. Distortion/smearing of the signal due to mixing, sensor response, or thermal inertia is always present, but it is important only if the response time of the apparatus is comparable to the duration of the event. For example, in fire calorimeter tests of lithium-ion batteries, the battery contents are ejected and burned in a matter of seconds, which is comparable to the cone calorimeter response time; the cone calorimeter (apparatus) cannot keep up with the dynamics of the event and the peak heat release rate (PHRR), $\dot{Q}_{max}$, is attenuated. Correcting the recorded data for distortion by the apparatus to capture the peak value of an event history is an important problem because the fire hazard is often proportional to the PHRR. The inverse problem is also important when comparing numerical predictions to test results. In this case, the computed event history (e.g., a ThermaKin or a computational fluid dynamics calculation) occurs in real time but must be intentionally distorted to approximate the apparatus response (test data).

The most general relationship between a recorded signal, θ, the event history to be measured, $dQ/dt = \dot{Q}(t)$, and the apparatus function, $K(t)$, is,

$$\theta(t) = \int_0^t \dot{Q}(x)K(t-x)dx \qquad \text{(A-1)}$$

Equation A-1 states that the apparatus response θ depends not only on the instantaneous value of $\dot{Q}$ at time t but also on the integrated effect, or complete history, of all past values of $\dot{Q}$. That is, the apparatus response to $\dot{Q}$ at the present time, $\theta(t)$, inherits the effects of all past actions of the apparatus over $(t-x)$. For this reason, equation A-1 is called a hereditary integral, and it describes an apparatus response that is cumulative in time. In this case, $\dot{Q}$ is usually the HRR; θ is a change in oxygen concentration or thermopile voltage; and the apparatus is usually an OSU fire test apparatus, a cone calorimeter, or a fire test. The most common response function is an exponential:

$$K(t) = \frac{C}{\tau} e^{-t/\tau} \qquad \text{(A-2)}$$

The constant C is the calibration factor and τ is the characteristic (response) time of the apparatus. Substituting equation A-2 into equation A-1:

$$\theta(t) = \frac{C}{\tau} \int_0^t \dot{Q}(x) e^{-\frac{(t-x)}{\tau}} dx \qquad \text{(A-3)}$$

Equation A-3 can be integrated analytically when $\dot{Q}(t) = \dot{Q}_0 = $ constant, as during a calibration:

$$\frac{\theta(t)}{C} = \dot{Q}_0 (1 - e^{-t/\tau}) \qquad \text{(A-4)}$$

Equation A-4 shows that when $t = \tau$, $\theta(t)/C = \theta(\tau)/C = \dot{Q}_0(1-e^{-1}) = 0.63\,\dot{Q}_0$; that is, the signal reaches 63% of the maximum steady-state response, $\theta(\infty)/C = \dot{Q}_0$, from which the value of the calibration constant is calculated, $C = \theta(\infty)/\dot{Q}_0$. Figure A-1 illustrates the apparatus response to a step change in $\dot{Q}$ from 0 to $\dot{Q}_0$ at $t = 0$ for an exponential apparatus function with $\tau = 10$s.
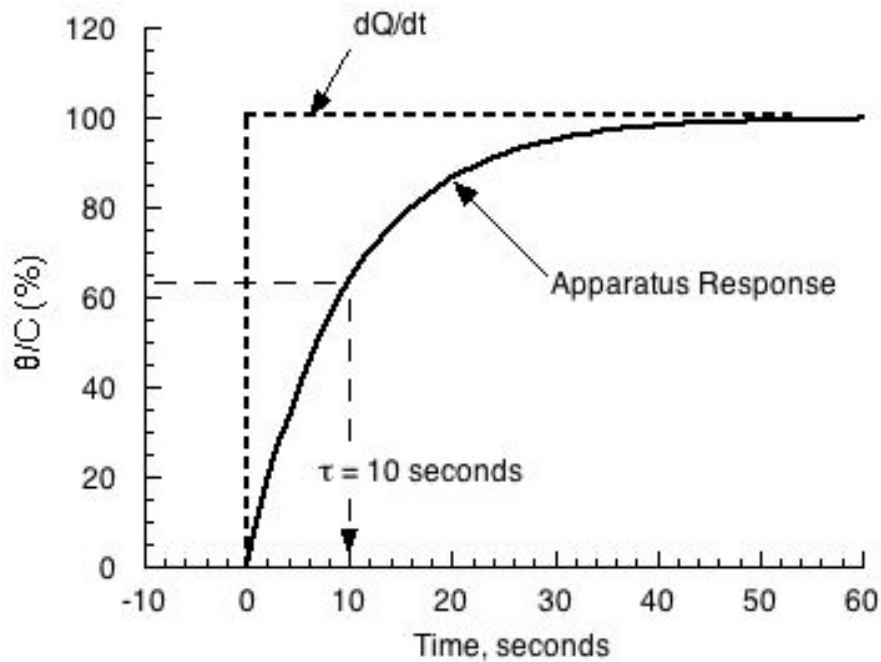
Figure A-1. Response of an apparatus with $\tau = 10$s to a constant HRR applied at $t = 0$

Equation A-3 is a hereditary integral that describes the measured signal θ in terms of the entire event history $\dot{Q}$. Equation A-3 can be inverted to express the event history $\dot{Q}$ in terms of the measured signal θ by differentiating both sides with respect to time and rearranging terms:

$$\dot{Q}(t) = \frac{1}{C}\left(\theta + \tau\frac{d\theta}{dt}\right) \qquad \text{(A-5)}$$

A-2

Equation A-5 shows that only if the apparatus response is infinitely fast ($\tau = 0$), or the signal reaches steady state ($d\theta/dt = 0$), does $\dot{Q}(t) = \theta(t)/C$. The HRR output of the apparatus is assumed to be $HRR \equiv \theta/C$, and it is related to the actual HRR in test $\dot{Q}$, as:

$$\dot{Q}(t) = \mathrm{HRR} + \tau\frac{d\mathrm{HRR}}{dt} \tag{A-6}$$

The heat released up to time t during the test is the integral of equation A-6:

$$Q(t) = \int_0^t \dot{Q}(x)\,dx = \int_0^t \mathrm{HRR}(x)\,dx + \tau\mathrm{HRR}(t) \tag{A-7}$$

The total heat of the burning process after HRR returns to zero following the event is independent of the test dynamics:

$$Q(\infty) = Q_{total} = \int_0^\infty \mathrm{HRR}(t)\,dt \tag{A-8}$$

The following sections are examples of the use of equations A-3 and A-6 to correct for the time-dependent apparatus response of test measurements.

CORRECTING TEST DATA FOR APPARATUS RESPONSE

FIRE CALORIMETER (CONE AND OSU) TESTS

Test data for a time-dependent event $\dot{Q}(t)$ can be corrected for smearing/distortion due to the apparatus response (deconvoluted) by using equation A-6. Operationally, the HRR vs. time data are differentiated to obtain $d\mathrm{HRR}/dt$ at each time t, which is multiplied by the time constant of the apparatus, τ, and then added to HRR. Figure A-2 is an example of a lithium-ion battery tested in a cone calorimeter, for which the time constant is $\tau = 3.3$ seconds.
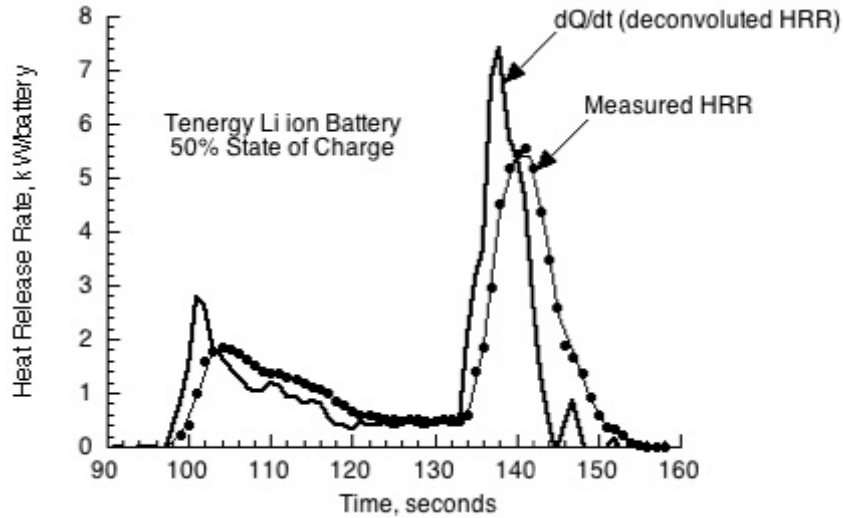
**Figure A-2. Deconvolution of cone calorimeter data for Tenergy lithium-ion battery
at 50 kW/m^2 external heat flux**

Because the duration of the battery HRR peak (5 seconds) is comparable to the response time of the cone calorimeter ($\tau = 3.3$ seconds), the measured signal must be deconvoluted using equation A-6 to obtain the PHRR. Correcting the HRR data for the apparatus response, shown as the solid line in figure A-2, reveals that the maximum HRR of the battery is significantly higher than the value reported by the apparatus (cone calorimeter).

FULL-SCALE TESTS

Deconvolution of full-scale fire test results is also useful when dilution and mixing of the combustion gases with fresh air causes distortion of the gas stream extracted from the test volume. Figure A-3 shows data from a fire test in the cargo compartment of the B707 test article in Building 275 (DOT/FAA/AR-TN05/9). In this experiment, propane was metered to a premixed burner and was calculated from the mass flow rate and the heat of combustion of propane assuming instantaneous and complete combustion. The characteristic time of the test was estimated from the flow rate of the exhaust (combustion) gases and the volume (V) of the compartment to be $\tau = V/ \approx 30$ minutes.
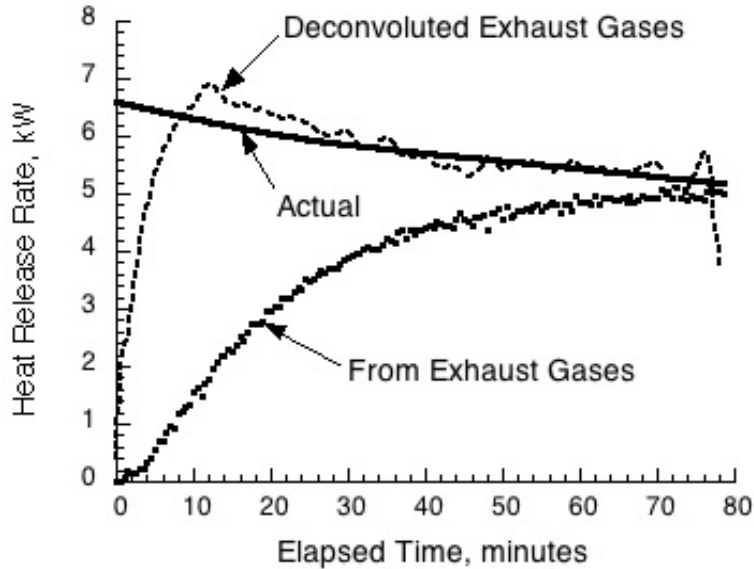
Figure A-3. Deconvolution of full-scale test data for HRR of propane burner in cargo compartment of B707 test article (actual HRR of propane burner [solid line], HRR calculated from exhaust/combustion gases [solid circles] and deconvoluted/corrected HRR [dashed line])

Figure A-3 shows the actual HRR of the propane burner and the HRR calculated from the oxygen depletion history of the exhaust gases drawn from the compartment using oxygen consumption calorimetry. Also shown in figure A-3 is $\dot{Q}$, obtained by deconvoluting these data using equation A-6 with $\tau = 30$s. The $\dot{Q}$ provides a much better approximation of the HRR of the burner than HRR computed directly from the combustion gases drawn from the compartment and better approximates the maximum value, $\dot{Q}_{max}$. The time constant due to compartment dilution and mixing with fresh air is very long (30 minutes), so short duration $\dot{Q}$ events (e.g., the step change in $\dot{Q}$ at $t = 0$) are poorly resolved by equation A-6.

COMPARING NUMERICAL SIMULATIONS TO TEST DATA

Numerical simulations of processes that occur in fire tests, $\dot{Q}$, are instantaneous ($\tau = 0$). To compare these simulations with test measurements in fire calorimeters or full-scale fire tests having a finite response time ($\tau > 0$), the computed event history $\dot{Q}(t)$ must be smeared (convoluted) to simulate HRR. Equation A-3 is used for this purpose in the form:

$$\text{HRR}(t) = \frac{\theta}{C} = \frac{e^{-t/\tau}}{\tau} \int_0^t \dot{Q}(x) e^{x/\tau} \, dx \tag{A-9}$$

Because exp[-t/τ] is not a function of the time variable of integration x, it comes outside of the integral in the last term of equation A-9. Equation A-9 can be evaluated in a spreadsheet by multiplying $\dot{Q}(t)$ by exp[t/τ] at each time t, integrating this product as a function of time, and

multiplying the resulting integral by $(C/\tau)\exp[-t/\tau]$ at each time t (i.e., by performing the numerical operations from right to left).

Figure A-4 shows a ThermaKin HRR simulation, $\dot{Q}$, of a single-ply epoxy-fiberglass fabric lamina tested in the OSU fire test apparatus as the dashed line. The experimental HRR by oxygen consumption is shown in the solid circles, and the solid line is HRR obtained by convoluting $\dot{Q}$ using equation A-9 with the measured $\tau = 5s$. The convoluted $\dot{Q}$ compares well with the measured HRR.
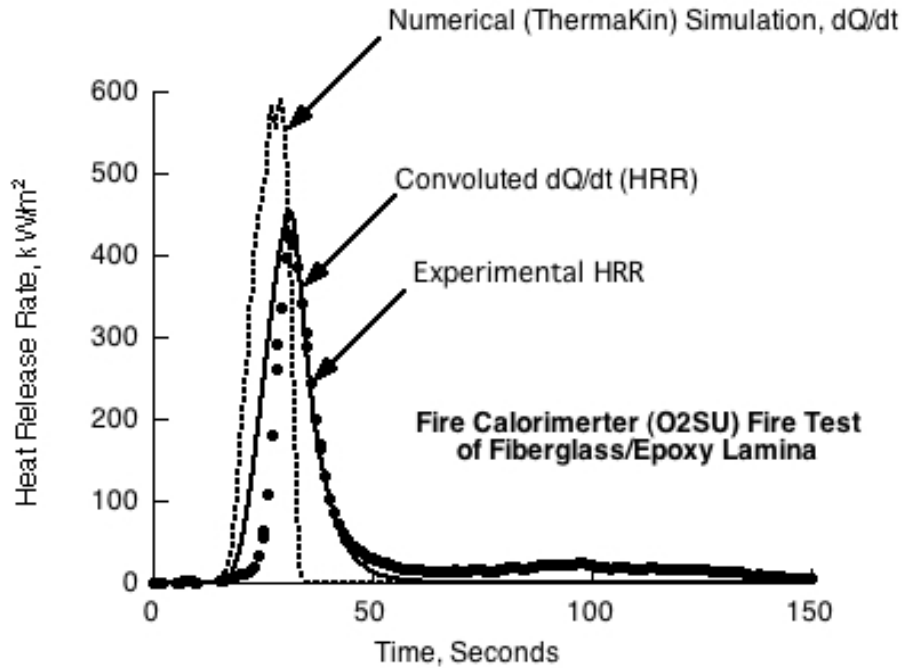
Figure A-4. Numerical simulation of the ignition and burning of a fiberglass/epoxy lamina (dashed line) as well as the convolution of this data using equation A-7 (solid line) compared to the measured apparatus response (solid circles)

APPENDIX B. HEAT CAPACITY OF THE 18650 BATTERY IN THE TEST SERIES

The specific heat of the battery was measured by using the data of Tests 22 and 24 up to approximately 200°C before any mass loss occurred. The process was calibrated by using an aluminum cylinder in place of the battery and adjusting the heat loss coefficient β (semi-infinite) through the insulation and electrical wires. A heat capacity was used of Al over the temperature range of interest as 1.05 J/g-K, as shown in Figure B-1.
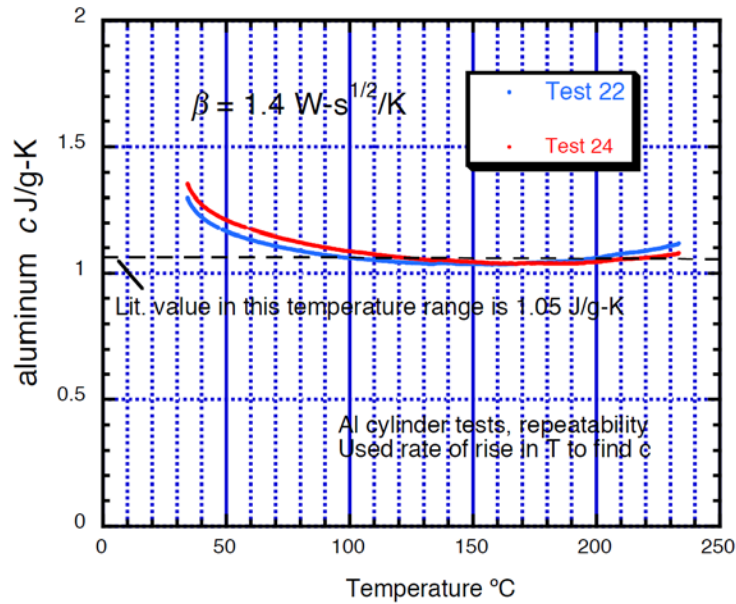
Figure B-1. Calibration of heat loss to obtain specific heat for aluminum

APPENDIX C. SUMMARY OF TESTS 27-34 AT 80% CHARGE

This section contains the detailed results of tests 27–34 for the decomposition calorimetry tests. These tests had 80% state of charge (SOC), and the power to initiate the thermal runaway was varied from approximately 3 W–74 W. The specific conditions of these tests are among those in table C-1. Though the table provides an overview of the test results for conditions of varying SOC and power, it is important to see the results presented over time (see figures C-1–C-8). Therefore, we list here the time behavior for tests 27–34.

Table C-1. Results of Tenergy 18650 lithium-ion battery thermal decomposition tests

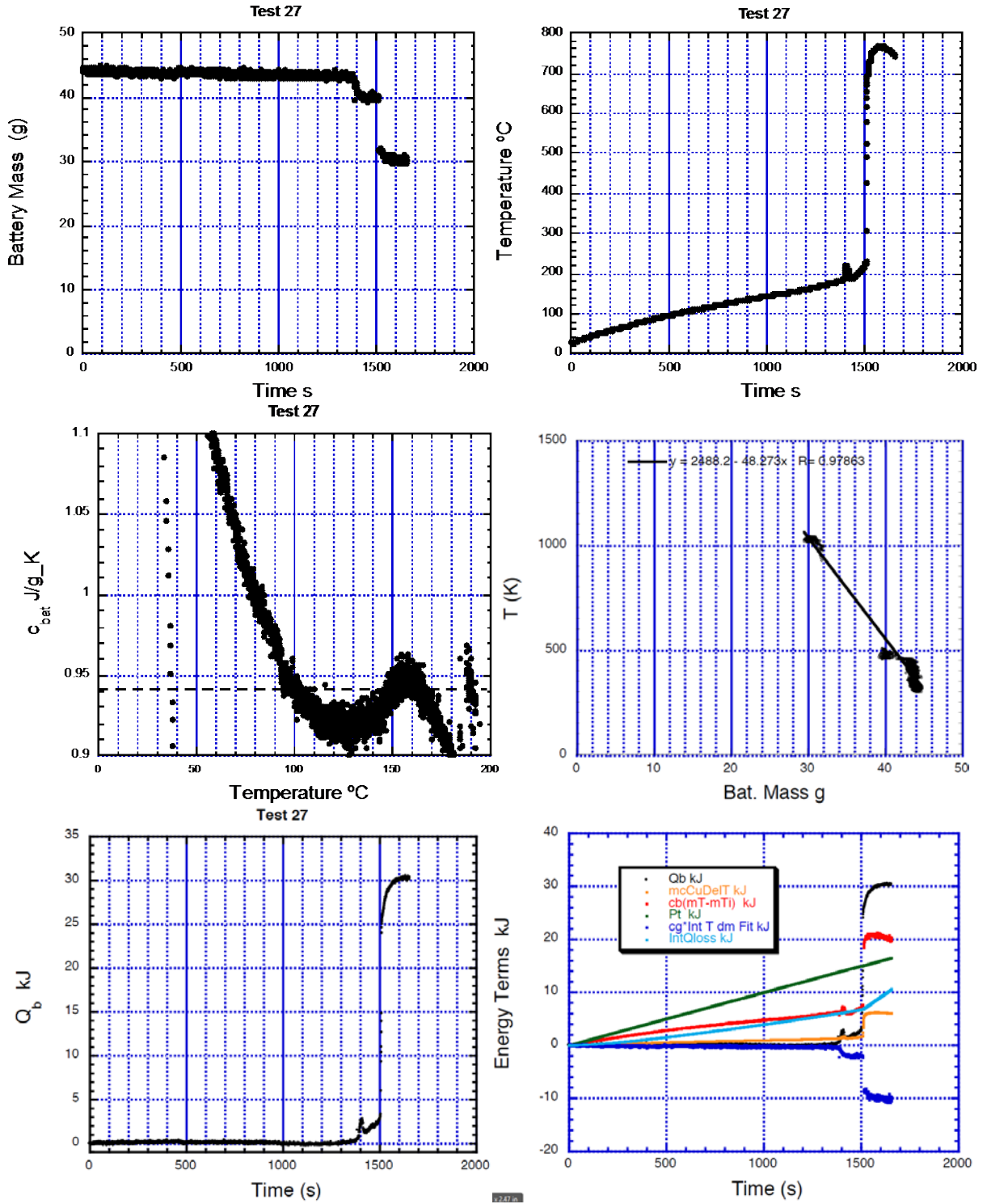| Test No	SOC %	P (W)	Init. Mass g	Time 1st vent s	Mass after 1st vent g	Time 2nd vent s	Mass after 2nd vent g	Final Mass g	T @ 1st vent °C	T @ 2nd vent °C	T_{max} °C	Q_b max kJ
9	0.5V	25.3	44.3	400	44	400	34	38.6	190	230	800	2
19	0	26.9	44	400	42	800	37	na	180	280	560	0
18	22	27.6	43.8	450	41	550	34	38.2	200	270	670	17
16	30	23.6	43.8	630	41	700	37	38.2	200	260	580	17
14	40	26.1	44.2	540	42	630	37	37.9	210	270	650	21
21	60	25.7	44	400	41	560	31	35.7	180	240	740	28
13	60	26.4	44.3	500	40	580	31	33.9	200	250	950	25
28	80	2.8	44	n/a	n/a	n/a	n/a	44	n/a	n/a	n/a	0
27	80	9.95	44.2	1380	40	1520	30	32.6	n/a	230	770	30
29	80	22.1	44.1	590	43	670	28	32.9	n/a	270	800	31
11	80	23.6	44.1	550	42	640	32	31.9	190	250	910	33
7	80	25.2	44.3	570	43	640	32	32.4	200	250	1350	40
8	80	25.2	44.2	440	40	540	29	31.7	200	250	840	33
30	80	36.4	44	350	40	395	31	30.6	n/a	260	830	32
31	80	49.5	44.2	220	38	270	28	32.8	n/a	270	870	33
32	80	58.8	44.1	174	40	220	31	32.1	n/a	280	820	28
33	80	73.2	44	130	41	165	25	30	n/a	n/a	n/a	n/a
34	80	74.2	44.1	125	40	165	29	32	n/a	270	930	35
25	90	26.4	n/a	n/a	n/a	n/a	n/a	na	n/a	n/a	n/a	n/a
23	90	27	44.1	500	42	550	25	25.9	200	240	640	20
15	100	25	44.3	520	41	570	29	27.5	200	250	800	31
12	100	25.5	44.3	540	41	600	n/a	29	n/a	n/a	1200	48
17	100	25.6	44.1	500	40	550	24	24.6	200	250	800	30
10	100	25.8	44.1	480	40	540	-4	21.9	190	250	n/a	n/a

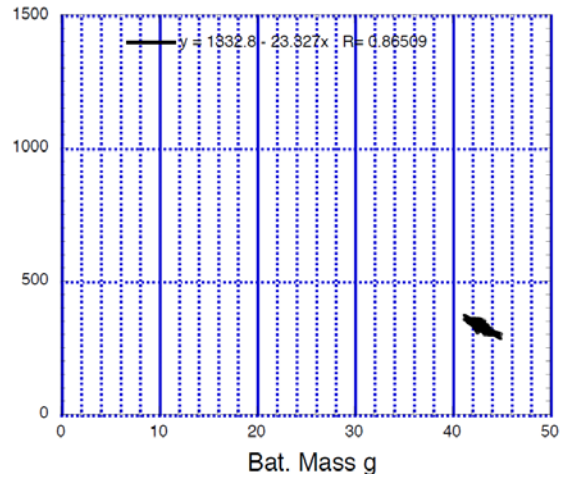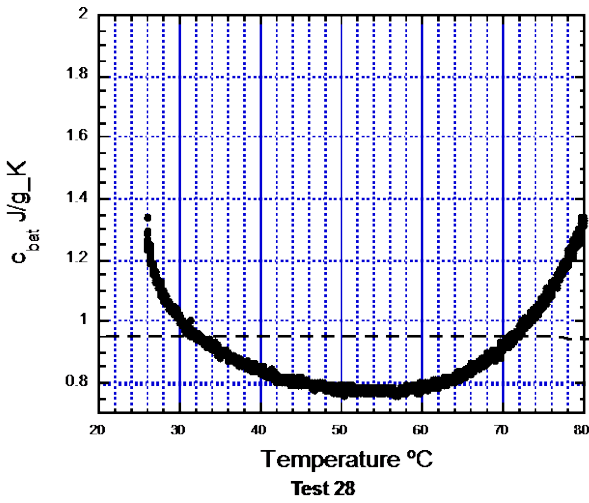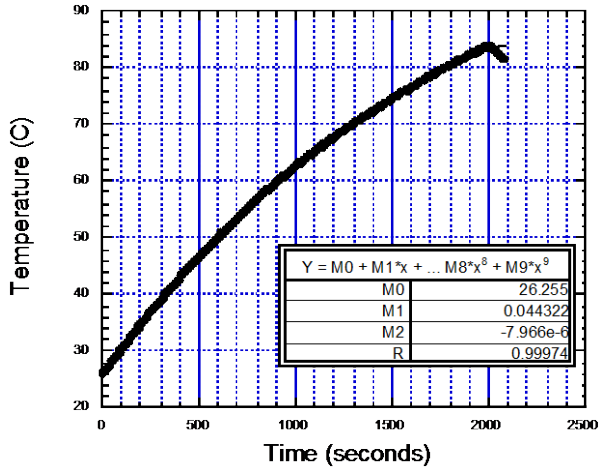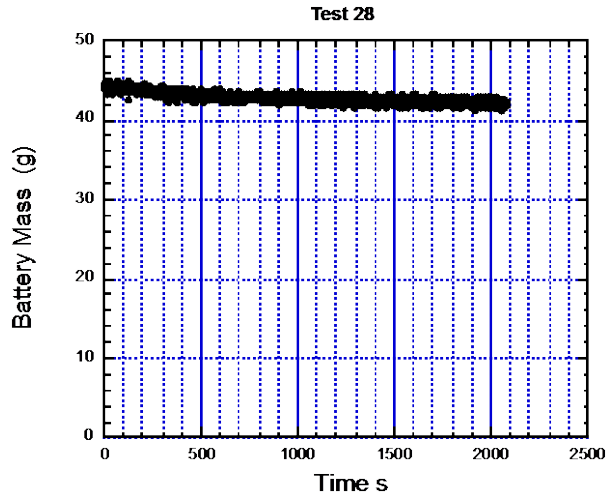**Figure C-1. Detailed results over time for test 27: 9.95 W, SOC 80%**
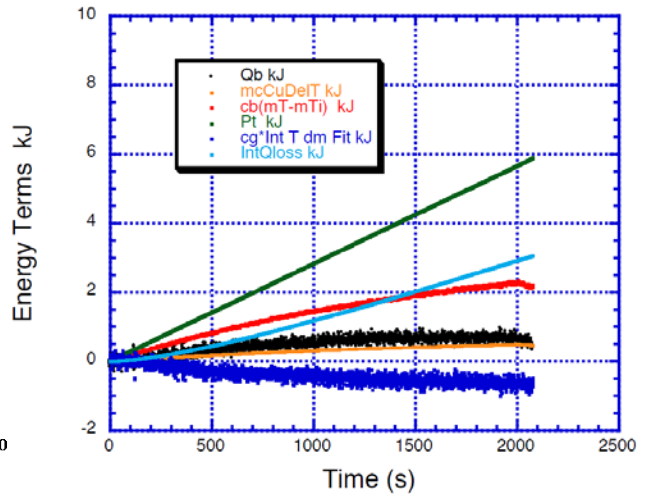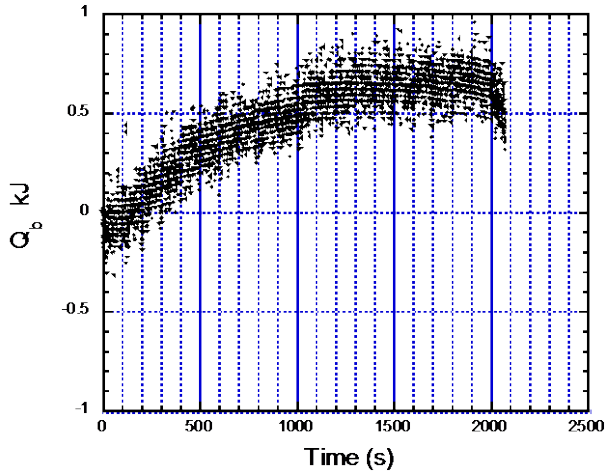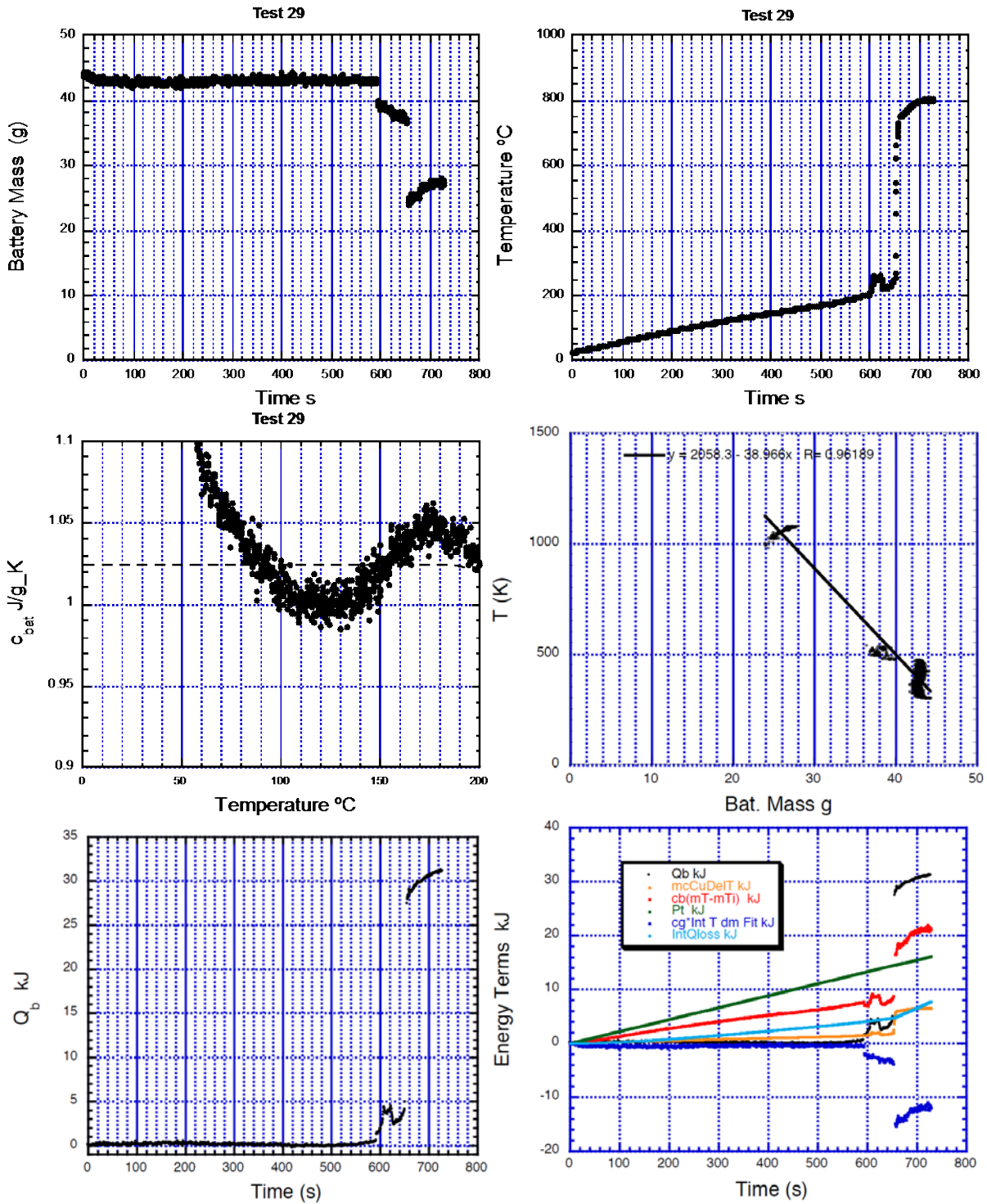
Figure C-2. Detailed results over time for test 28: 2.8 W, SOC 80%

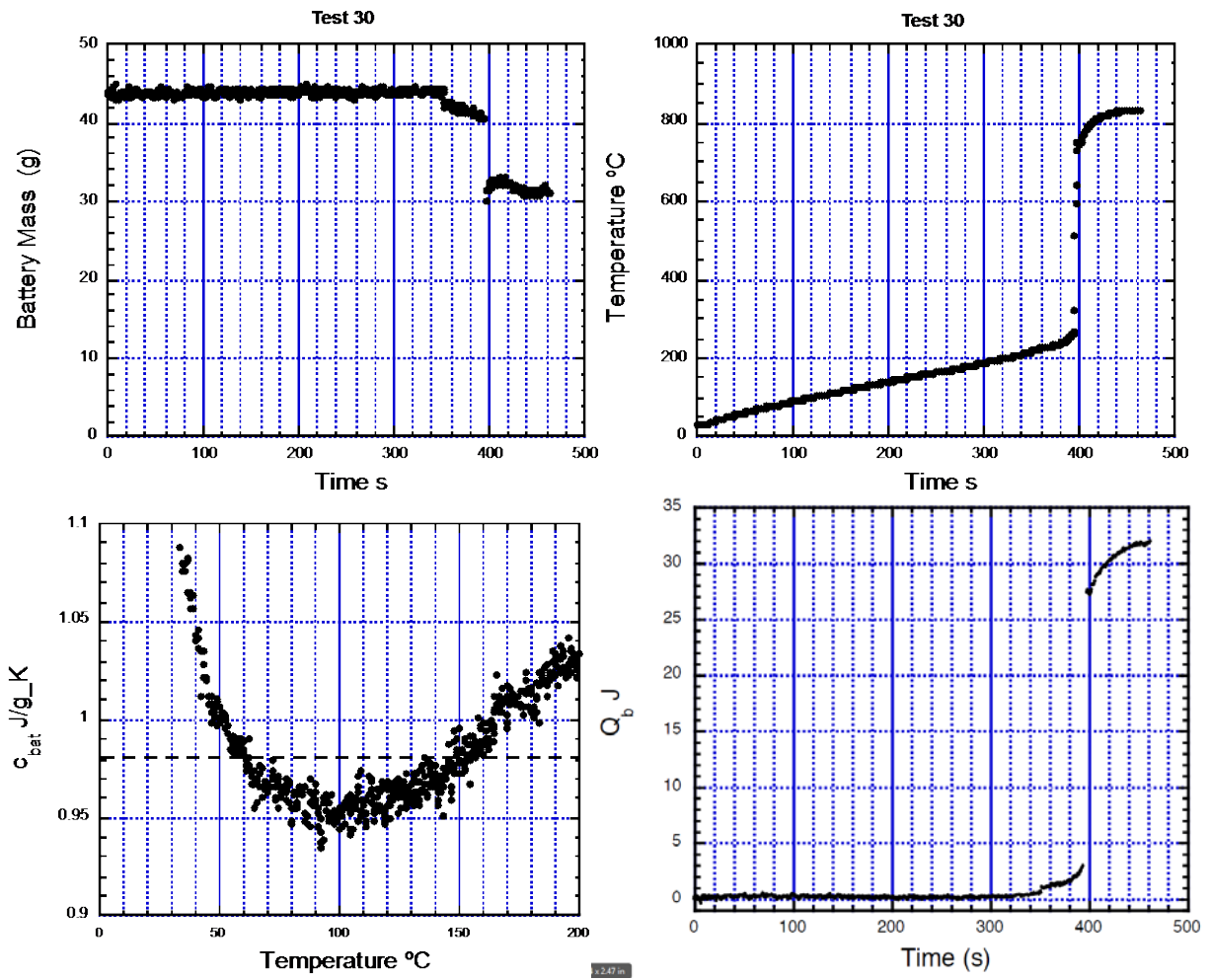**Figure C-3. Detailed results over time for test 29: 22.1 W, SOC 80%**

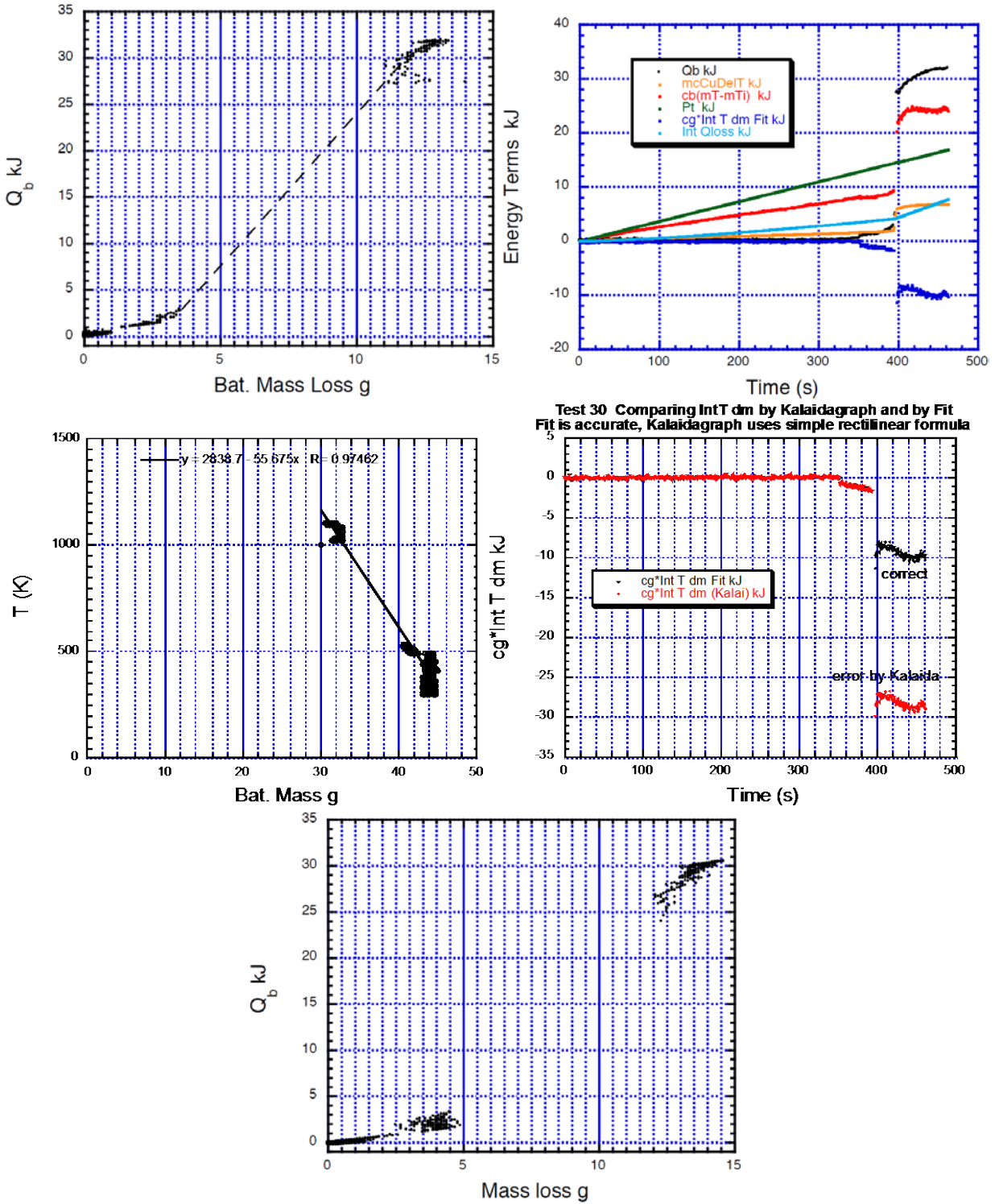**Figure C-4 Detailed results over time for test 30: 36.4 W, SOC 80%**

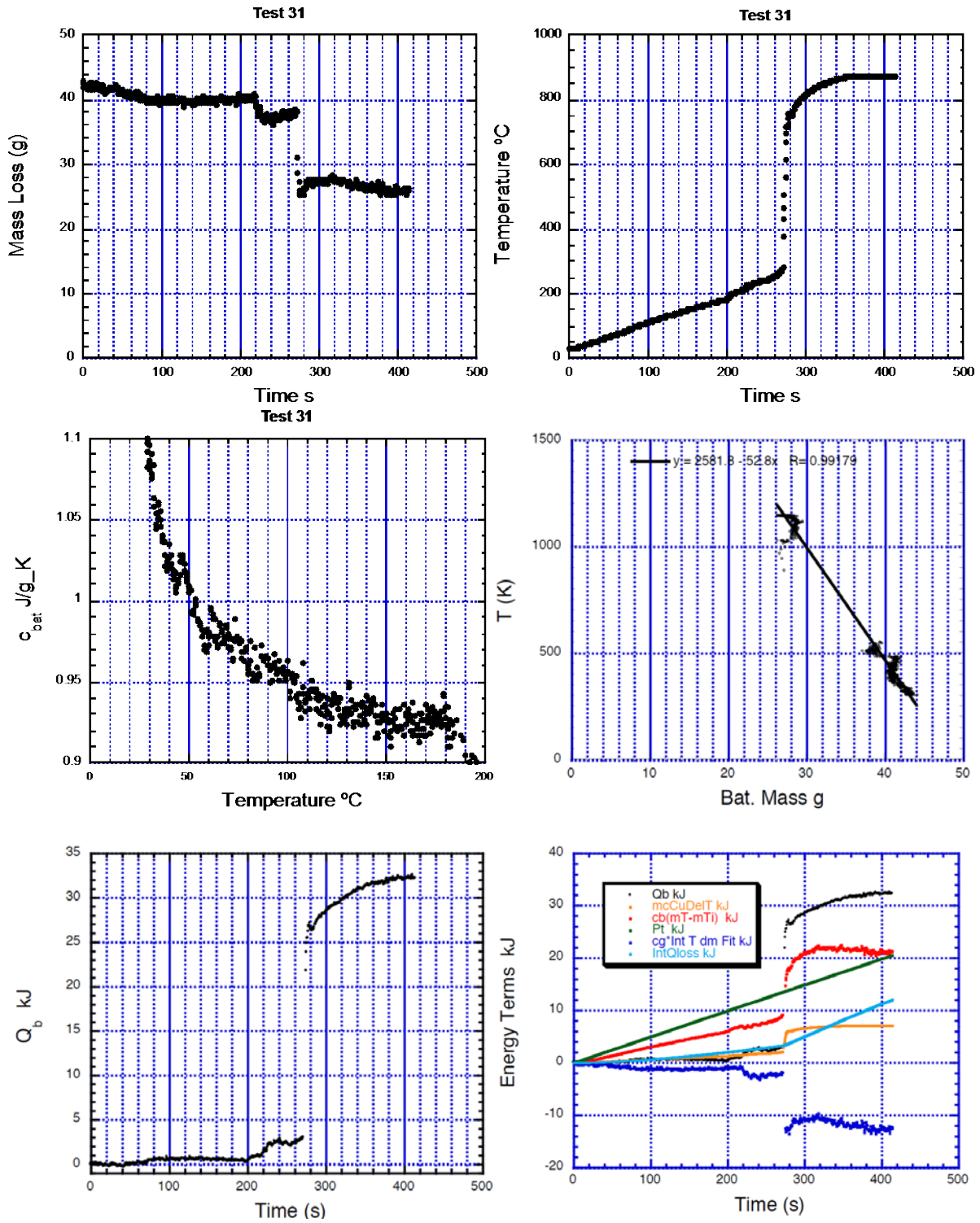**Figure C-4 Detailed results over time for test 30: 36.4 W, SOC 80% (continued)**

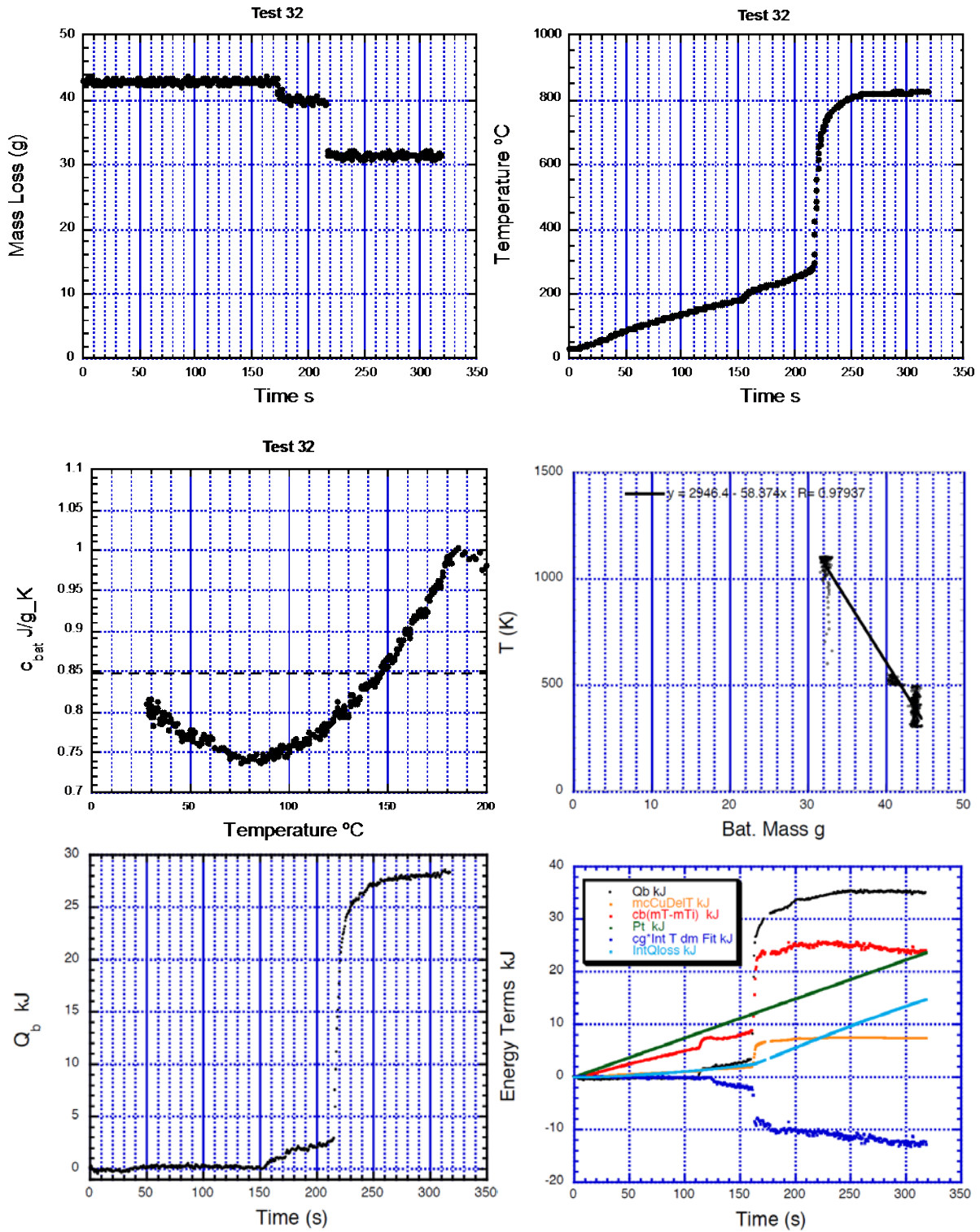**Figure C-5. Detailed results over time for test 31: 49. 5 W, SOC 80%**

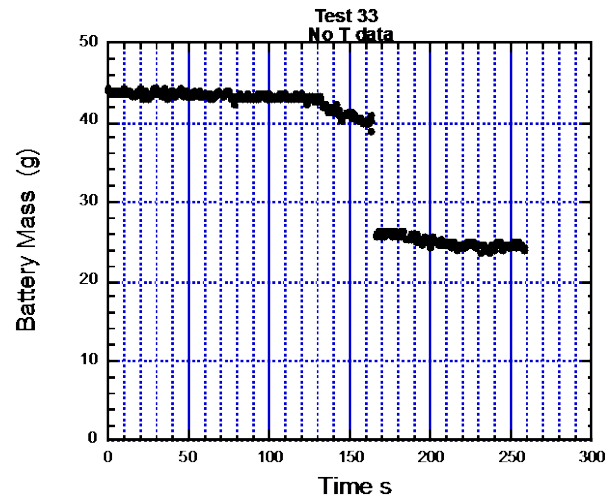**Figure C-6. Detailed results over time for test 32: 58.8 W, SOC 80%**

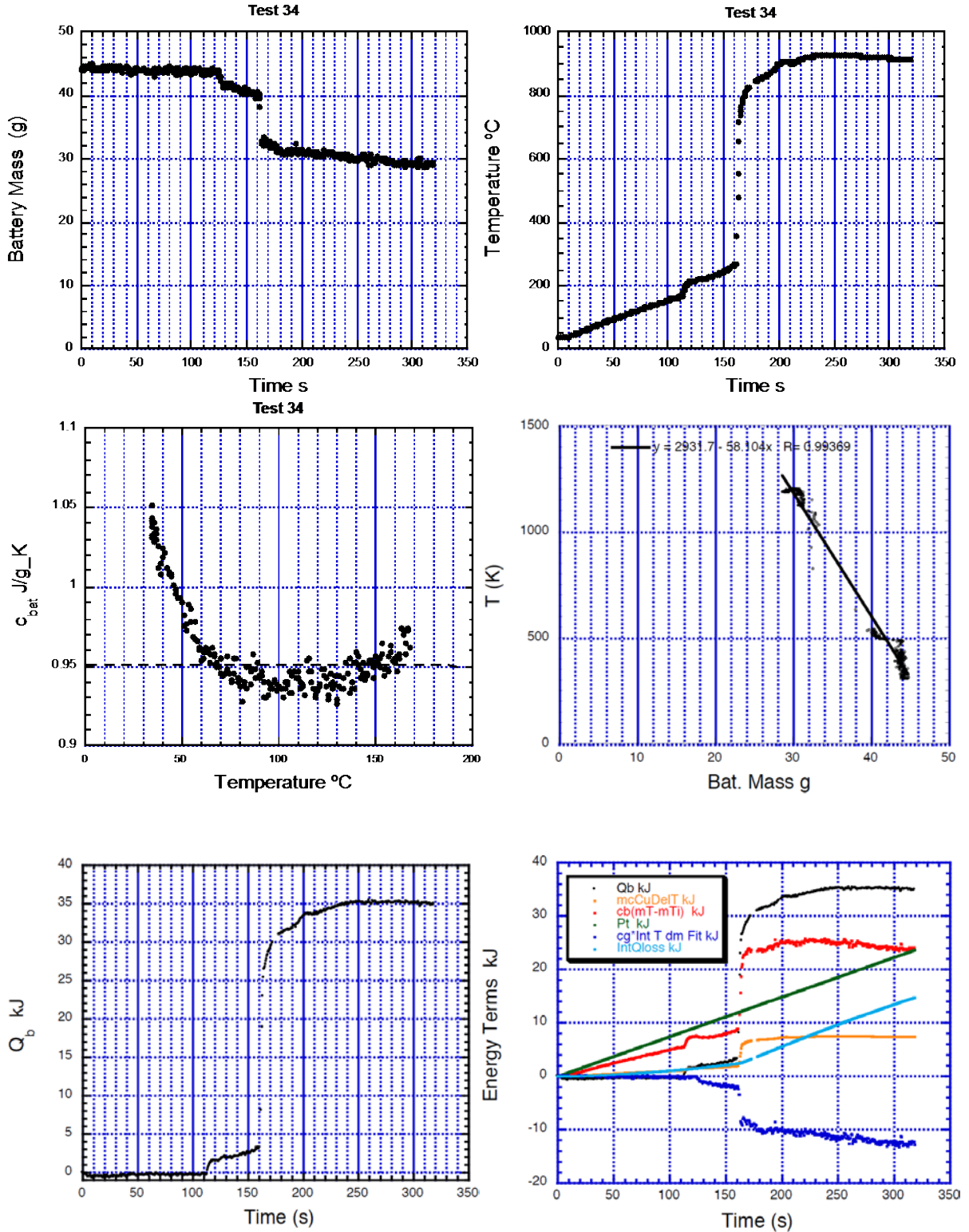**Figure C-7. Detailed results over time for test 33: 73.2 W, SOC 80%**

Figure C-8. Detailed results over time for test 34: 74.2 W, SOC 80%